RSC Advances

PAPER

View Article Online
View Journal | View Issue

Check for updates

Cite this: *RSC Adv.*, 2025, **15**, 21987

Efficient Schiff base ligand for selective Cd(II) and Pb(II) removal from water†

Amal E. Mubark, *[a] Sabreen M. El-Gamasy,[b] Ahmed M. Masoud, [a] Adel A. El-Zahhar, [c] Majed M. Alghamdi,[c] Mohamed H. Taha [a] and Taha F. Hassanein[d]

Received 30th April 2025
Accepted 23rd June 2025

DOI: 10.1039/d5ra03053f

rsc.li/rsc-advances

This study reports the development and evaluation of a novel Schiff base ligand, 2-((*E*)-(4-aminophenylimino)methyl)benzoic acid, for the efficient removal of lead(II) and cadmium(II) from aqueous solutions. The ligand was synthesized *via* a simple condensation route and characterized to confirm its structural and functional properties. Batch adsorption experiments were performed to investigate the effects of pH, temperature, metal ion concentration, contact time, and competing ions. The ligand exhibited high sorption capacities—84.0 mg g^{-1} for Pb(II) and 71.0 mg g^{-1} for Cd(II)—with optimal performance at pH 6.0. Adsorption kinetics followed a pseudo-second-order model, while equilibrium data fit well with the Langmuir and Sips isotherms, indicating chemisorption and monolayer coverage. Thermodynamic analysis confirmed the spontaneous and exothermic nature of the process. The ligand demonstrated excellent reusability over multiple cycles and retained strong selectivity in the presence of competing ions and in real wastewater. These findings suggest that the synthesized ligand is a promising and sustainable candidate for heavy metal remediation in water treatment applications.

1. Introduction

Water contamination by toxic elements, such as lead(II), and cadmium(II) poses a significant global environmental and public health challenge.[1–3] These pollutants are primarily introduced into water systems through industrial activities, including electroplating, battery manufacturing, and mining, as well as agricultural runoff containing fertilizers and pesticides.[1–5] Heavy metals, unlike organic pollutants, do not break down naturally, allowing them to remain in the environment for long durations. This persistence results in their buildup in aquatic systems and subsequent amplification in the food chain, creating significant health hazards for both humans and wildlife.[6–8] Chronic exposure to lead(II), and cadmium(II) has been linked to kidney dysfunction, bone demineralization, neurological disorders, and carcinogenic effects. In light of these risks, the World Health Organization (WHO) has set strict limits for the presence of these metals in drinking water, with allowable concentrations of 0.01, and 0.003 mg L^{-1} for lead and cadmium ions.[2,3] These standards highlight the critical need for effective, selective, and sustainable techniques for eliminating these pollutants from contaminated water sources.

Among the various remediation strategies, adsorption has gained recognition as a highly efficient method due to its ease of application, affordability, and remarkable removal efficiency.[9–13] The effectiveness of this approach is largely influenced by the selection of the ligand. Conventional sorbents, such as activated carbon,[14,15] clay minerals,[16,17] and zeolites,[18] have been widely used due to their large surface areas and low production costs. However, these materials often exhibit limitations, including low selectivity and reduced efficiency in the presence of competing ions.[19–21] To overcome these challenges, scientists have explored the use of advanced materials such as metal–organic frameworks (MOFs), biochar, and functionalized polymers. MOFs, characterized by their tunable pore sizes and functionalized surfaces, have shown excellent adsorption capacities for heavy metals like Pb^{2+}, Hg^{2+}, Cd^{2+}, and Cu^{2+}.[22] Similarly, biochar produced from agricultural residues is recognized for its eco-friendliness and high adsorption efficiency for Cd(II) under optimized conditions.[1] Functionalized polymers, engineered with chelating groups such as thiols and amines, provide targeted binding sites, enhancing the adsorption efficiency for specific metal ions.[23] Despite these advancements, there remains a pressing need for materials that are both cost-effective and highly selective, driving interest in the use of Schiff base ligands.

Schiff base ligands are recognized for their capacity to create stable complexes with metal ions, making them a focus of

[a]*Nuclear Materials Authority, P.O. Box 530, El Maddi, Cairo, Egypt. E-mail: amal_mubark2014@yahoo.com*

[b]*Chemistry Department, Faculty of Science, Menoufia University, Shebin El-Koam, 00123, Egypt*

[c]*Department of Chemistry, Faculty of Science, King Khalid University, P.O.Box 9004, Abha 61413, Saudi Arabia*

[d]*Chemistry Department, Faculty of Science, Helwan University, Helwan, Cairo, 11795, Egypt*

† Electronic supplementary information (ESI) available. See DOI: https://doi.org/10.1039/d5ra03053f

Open Access Article. Published on 27 June 2025. Downloaded on 2/9/2026 7:51:31 PM. This article is licensed under a Creative Commons Attribution-NonCommercial 3.0 Unported Licence.

Open Access Article. Published on 27 June 2025. Downloaded on 2/9/2026 7:51:31 PM. This article is licensed under a Creative Commons Attribution-NonCommercial 3.0 Unported Licence.

interest as effective ligands for extracting heavy metals from water.[9–12] These ligands can be tailored to improve selectivity and capacity for specific metal ions, making them versatile tools in environmental remediation. For example, Schiff base ligands derived from salicylaldehyde and *o*-phenylenediamine have been used to form complexes with Cd(II) ions, achieving adsorption efficiencies between 78% and 98% depending on the ligand structure.[6] Chitosan modified with bidentate Schiff base ligands has exhibited notable efficiency in removing Pb^{2+}, Cd^{2+}, and Cu^{2+} ions from water resources.[12] Additionally, chitosan enhanced with Schiff base ligands, such as 2(piperazin-1-yl)ethan-1-imine methyl benzaldehyde, has demonstrated a high adsorption efficiency for Pb(II) ions.[9] Schiff base- MOFs have also been recognized due to their selective adsorption of divalent metal ions, including Cd(II) and Pb(II).[24]

Although Schiff base-based ligands show great potential, challenges related to their regeneration and possible environmental impacts must be discussed. Future studies could aim to improve reusability and eco-friendliness of these materials to ensure sustainable application in water treatment processes. This research emphasizes the synthesis and characterization of a novel Schiff base ligand, 2-((*E*)-(4-aminophenylimino)methyl) benzoic acid, designed for the capture of lead(II) and cadmium(II) from aqueous solution. Ligand's structural and functional properties were characterized using techniques such as mass spectrometry, 1H-NMR, and IR spectroscopy, providing detailed insights into its adsorption mechanisms. Key variables, including solution pH, sorbent dosage, and adsorption properties, including thermodynamics, isotherms, and kinetics, were thoroughly examined to optimize the ligand's performance. This research not only highlights the ligand's efficiency and applicability but also contributes to the broader development of sustainable materials for environmental remediation.

2. Experiments

2.1. Materials

All chemicals were highly grade and employed in this investigation without additional purification. Cadmium sulfate ($CdSO_4$) and lead sulfate ($PbSO_4$) were utilized to prepare the stock solutions of Cd^{2+} and Pb^{2+} ions using double-distilled water. The synthesis of the Schiff base ligand, 2-((*E*)-(4-aminophenylimino)methyl)benzoic acid, was carried out using phthalic acid ($C_8H_6O_4$, 99.9%), *p*-phenylenediamine ($C_6H_8N_2$, 99.9%), and ethanol (95%), with phosphorus pentoxide (P_4O_{10}) employed as a drying agent. All reagents were sourced from Sigma-Aldrich, UK. Additionally, high-purity sulfuric acid (H_2SO_4), hydrochloric acid (HCl), and nitric acid (HNO_3), obtained from Merck, Germany, were used for the desorption process, facilitating metal ion recovery and ligand regeneration.

2.2. Synthesis of the ligand

The Schiff base ligand, 2-((*E*)-(4-aminophenylimino)methyl) benzoic acid, was synthesized through a straightforward and scalable condensation reaction between phthalic acid and *p*-phenylenediamine, following a well-established protocol for Schiff base formation.[25,26] This synthesis route was chosen for its simplicity, high yield, and ability to produce a ligand with well-defined functional groups suitable for heavy metal adsorption. In a typical procedure, equimolar amounts of phthalic acid (5 g, 0.0301 mol) and *p*-phenylenediamine (3.254 g, 0.0301 mol) were dissolved in 95% ethanol. The mixture was refluxed under continuous stirring for six hours to ensure complete reaction. The reaction progress was tracked using thin-layer chromatography (TLC), which confirmed the full consumption of the starting materials.[27,28] Once cooled to room temperature, the ligand solidified and was subsequently washed with ethanol to eliminate any unreacted precursors and byproducts. The purified product was dried in a vacuum desiccator over phosphorus pentoxide (P_4O_{10}), yielding a high-purity ligand suitable for adsorption studies.[29] The synthetic pathway for the ligand preparation is illustrated in Fig. 1.

2.3. Ligand characterization

A variety of analytical techniques were employed to investigate the morphology, structure, and surface properties of the synthesized ligand. Details of the instruments used for these

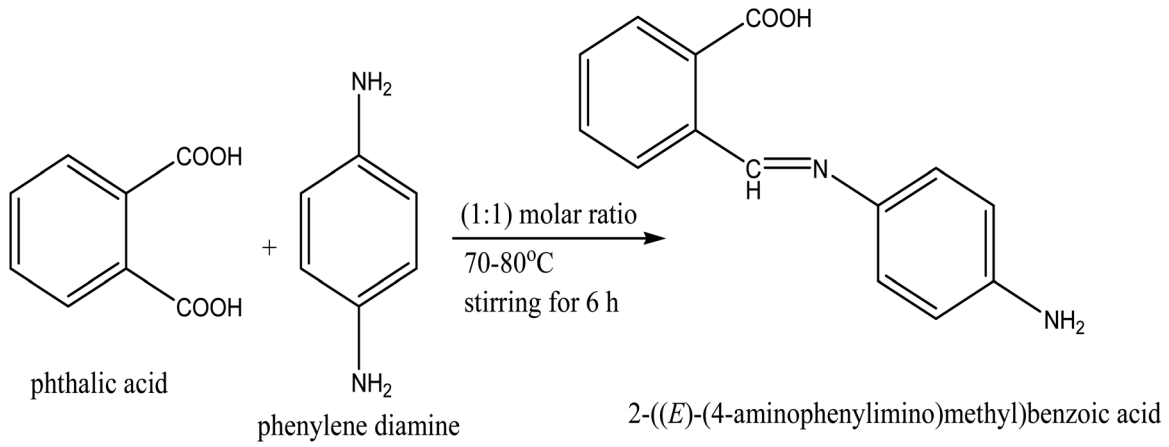

Fig. 1 Schematic representation of the synthesis of 2-((*E*)-(4-aminophenylimino)methyl)benzoic acid.

© 2025 The Author(s). Published by the Royal Society of Chemistry

Open Access Article. Published on 27 June 2025. Downloaded on 2/9/2026 7:51:31 PM. This article is licensed under a Creative Commons Attribution-NonCommercial 3.0 Unported Licence.

analyses can be found in Section S1† of the complementary materials accompanying this article.

2.4. Adsorption experiments

The effectiveness of 2/(*E*)-(4-aminophenylimino)methyl)benzoic acid in removing cadmium(II) and lead(II) from aqueous solution was assessed by batch adsorption tests. Utilizing a Scientific Precision Thermo-shaker water bath (model: SWB 27, USA), these tests were conducted in polypropylene tubes. A specific amount of the ligand (m, g) was added to a known volume (V, L) of a metal ion solution with a 50 mg L^{-1} as original concentration (Co, mg L^{-1}). The mixture was shaken at 25 ± 1 °C for 600 minutes to reach equilibrium. Parameters such as solution pH (2–9) and ligand dose (1.0–5.0 g L^{-1}) were adjusted to identify the best adsorption conditions. To test the ligand's reusability, desorption experiments were conducted. The metal-loaded ligand was treated with different eluents (nitric acid, hydrochloric acid, or sulfuric acid) for 10 hours at an ligand dose of 4.0 g L^{-1}. Desorption efficiency was measured by analyzing the eluate.

The adsorption kinetics were studied by adjusting the shaking time from 5 to 600 minutes. Three conventional kinetic models (*i.e.* Elovich, pseudo-second-order, pseudo-first-order (Lagergren), and Weber and Morris) were employed for analyzing the anticipated experimental data. For adsorption isotherms, tests were performed with initial metal ion concentrations in the range of 20 to 200 mg L^{-1}. Common isotherm models (*i.e.* Sips, Temkin, Freundlich, and Langmuir) were employed for evaluating the obtained data. The non-linear forms of these models are presented in Table S1†.[30–38] The average relative error (ARE) and the coefficient of determination (R^2) were applied to fitting the accuracy of each model, as outlined in Table S1†.[30,31,37] Thermodynamic properties, including the standard entropy change ($\Delta S°$), standard enthalpy change ($\Delta H°$), and standard Gibbs free energy change ($\Delta G°$), were determined across a temperature range of 25 to 50 ± 1 °C. These parameters were obtained using the equations provided in Table S1† (ref. 31 and 39) and offered insights into the feasibility and spontaneity of the uptake system.

Atomic Absorption Spectrometer (GBC 932 AA, UK) was engaged for determining the initial (C_o) and equilibrium (C_e) concentrations of cadmium and lead ions. Before analysis, a 0.22 μm filters were utilized for samples filtration to eliminate any particulate matter. All experiments were conducted in triplicate, and results with a relative error of ≤5% were considered adequate. The adsorption efficiency (E%), adsorption capacity (q_o, mg g^{-1}), and distribution coefficient (K_d) were calculated using the following equations:

$$q_e = (C_o - C_e) \times \frac{V}{m} \quad (1)$$

$$R\% = \frac{(C_o - C_e)}{C_o} \times 100 \quad (2)$$

$$K_d = \frac{q_e}{C_e} \times 100 \quad (3)$$

3. Results & discussion

3.1 Characterizations of the ligand

The prepared ligand, 2-((*E*)-(4-aminophenylimino)methyl)benzoic acid, was characterized to validate its structural integrity, purity, and chemical properties. As a Schiff base derived from the condensation of 4-aminobenzaldehyde and 2-carboxybenzaldehyde, its structural attributes were examined using multiple analytical techniques.

3.1.1. Elemental analysis and molecular composition. The ligand was obtained as a black solid with a melting point of 210 °C, indicating high thermal stability—a desirable property for ligands used in coordination chemistry. The synthesis yielded 75%, demonstrating an efficient synthetic procedure with minimal loss, which further attests to the robustness of the synthetic route. Elemental analysis provided critical confirmation of the ligand's molecular composition, with experimentally determined percentages of carbon (70.32%), hydrogen (5.18%), and nitrogen (11.23%) closely matching the calculated values (69.99%, 5.03%, and 11.32%, respectively). This close agreement confirms the high purity of the ligand and validates its proposed molecular formula, $C_{14}H_{12}N_2O_2$. The existing oxygen and nitrogen in the ligand's structure is particularly significant, as these elements are associated with functional groups like –NH_2 (amino) and –COOH (carboxyl), that essential for metal ion coordination and adsorption.

3.1.2. Mass spectrometry. Mass spectrometry (MS) played a pivotal role in confirming the molecular structure and assessing the stability of the synthesized ligand, 2-((*E*)-(4-aminophenylimino)methyl)benzoic acid.[40,41] A mechanistically grounded fragmentation pathway has been proposed (Fig. 2) based on the ligand's structural features and established MS fragmentation rules for Schiff bases. The first key fragmentation step involves the loss of the carboxyl group (–COOH), which is thermodynamically favorable and commonly observed in carboxylic acid derivatives. This decarboxylation produces a stable aromatic intermediate, retaining the aminophenylimino core. Subsequently, cleavage near the imine (–C=N–) linkage results in the formation of a secondary fragment *via* the elimination of a C_4H_3N moiety, consistent with the known lability of imine bonds under ionizing conditions. The resulting species contain aromatic structures stabilized by resonance and electron delocalization, which is typical of fragmentation in conjugated systems.

The generation of these fragments supports the presence of core functional groups—particularly –COOH, –NH_2, and –C=N—that are directly involved in adsorption mechanisms. Their stability during fragmentation further suggests that these moieties form robust coordination sites, aligning with the observed high affinity of the ligand for divalent metal ions such as Pb(II) and Cd(II). The proposed fragmentation behavior (Fig. 2) thus provides indirect but valuable structural validation. It also offers mechanistic insight into the potential electron-donating sites that govern the ligand's interaction with metal ions during adsorption. These observations reinforce the

Open Access Article. Published on 27 June 2025. Downloaded on 2/9/2026 7:51:31 PM.
This article is licensed under a Creative Commons Attribution-NonCommercial 3.0 Unported Licence.

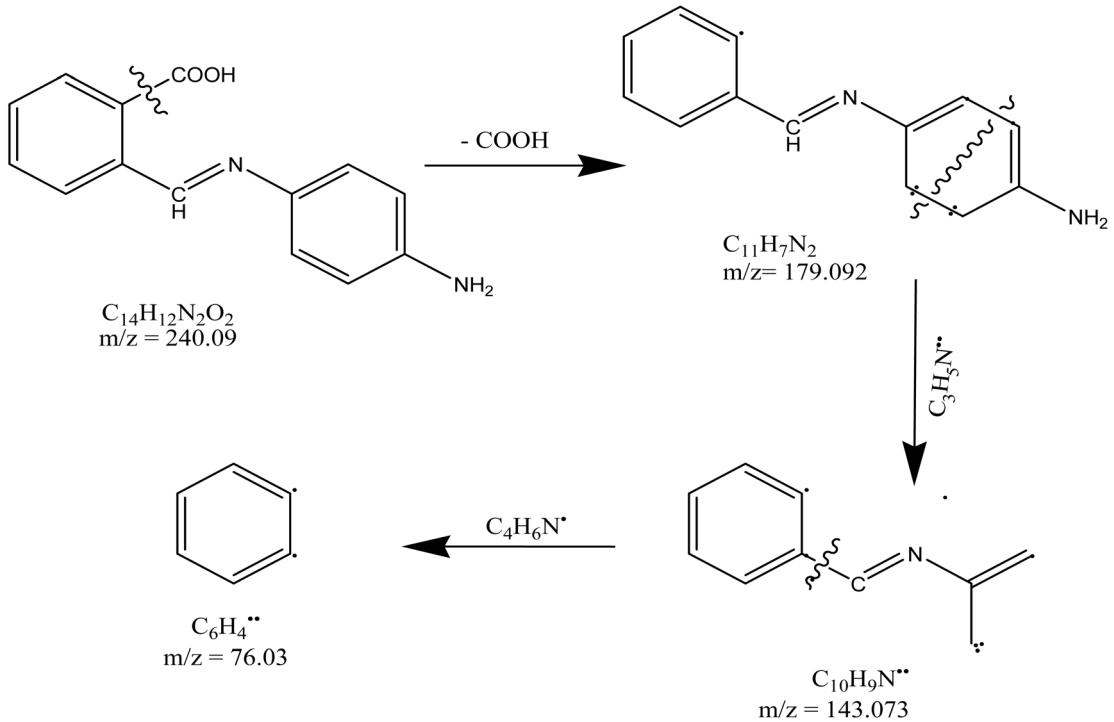

Fig. 2 Proposed fragmentation pathway of 2-((*E*)-(4-aminophenylimino)methyl)benzoic acid.

suitability of this Schiff base framework for applications in selective heavy metal capture from aqueous environments.

3.1.3. Infrared spectroscopy (IR). FTIR spectral analysis of the ligand before and after adsorption provides valuable insights into its structural integrity and metal-binding interactions (Fig. 3). Initially, the spectrum highlights key functional groups responsible for adsorption. The amino group stretching vibrations (ν(NH)) appear at 3280 cm^{-1} and 3150 cm^{-1}, while broad absorptions in the 3410–3180 cm^{-1} and 3160–2750 cm^{-1} regions indicate extensive intra- and intermolecular hydrogen bonding, which are essential for the stabilization of the ligand and facilitating metal ion coordination.[23,24] The presence of strong bands at 1735 cm^{-1} (νC=O) and 1617 cm^{-1} (νC=N) confirms the Schiff base structure, reinforcing its chelation ability. Additionally, aromatic ring vibrations at 1620 cm^{-1}, 1590 cm^{-1}, and 750 cm^{-1} validate the structural integrity of the ligand, further supporting its potential as an effective ligand[23,24](Fig. 3).

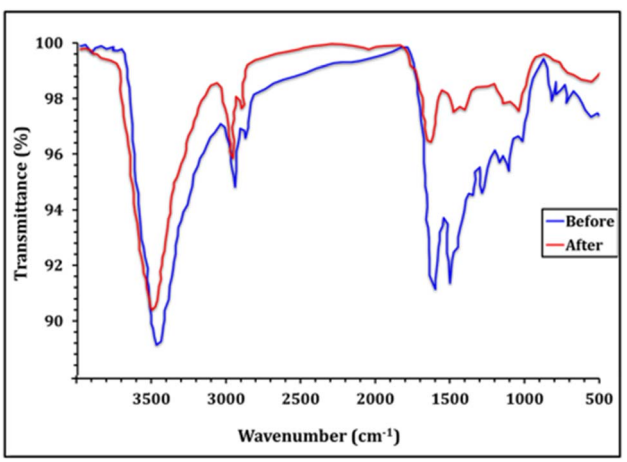

Fig. 3 IR spectrum with key functional group vibrations before (I) and after (II) adsorption process.

Upon adsorption, notable spectral shifts and intensity changes occur, reflecting metal–ligand interactions. The ν(NH) bands show slight shifts and reduced intensity, suggesting direct involvement of the amino group in coordination. The ν(C=O) stretching vibration, originally at 1735 cm^{-1}, shifts to a lower wavenumber, indicating metal binding through the carbonyl oxygen. Similarly, the ν(C=N) band at 1617 cm^{-1} undergoes a shift, confirming the participation of imine nitrogen in metal complexation. These spectral modifications highlight the primary role of Schiff base functional groups in lead(II) and cadmium(II) capture (Fig. 3).

While the characteristic aromatic ring vibrations remain visible, minor shifts and intensity variations suggest subtle electronic effects or conformational adjustments following metal binding. Despite these changes, the ligand maintains its fundamental structural features, reinforcing its stability during the adsorption process. The persistence of broad hydrogen-bonding regions suggests that hydrogen bonding still contributes to the adsorption mechanism alongside direct metal coordination. These spectral observations collectively confirm the ligand's strong tendency for cadmium(II) and lead(II), highlighting its suitability for recycle in wastewater treatment applications.

© 2025 The Author(s). Published by the Royal Society of Chemistry

Open Access Article. Published on 27 June 2025. Downloaded on 2/9/2026 7:51:31 PM.
This article is licensed under a Creative Commons Attribution-NonCommercial 3.0 Unported Licence.

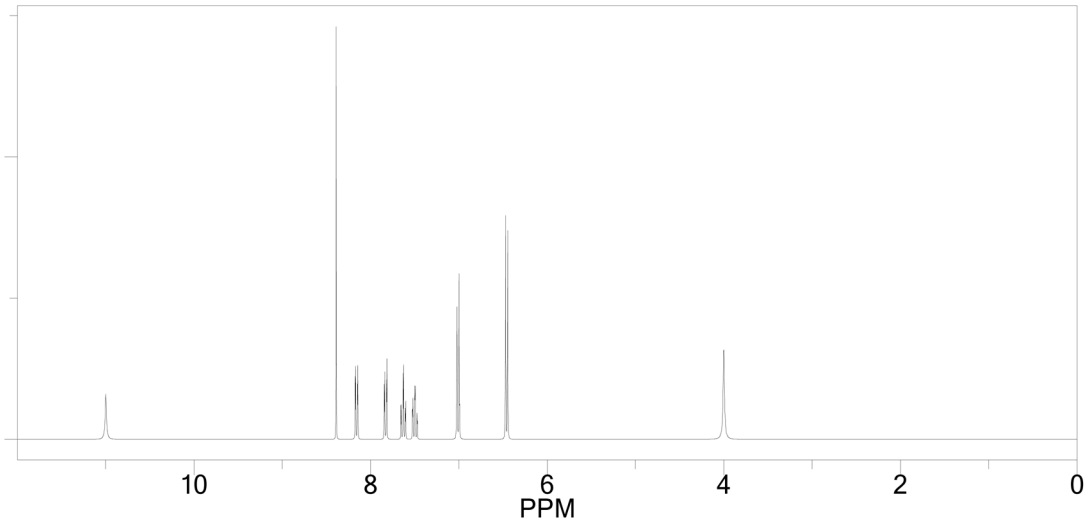

Fig. 4 ^{1}H-NMR spectrum of the ligand.

3.1.4. ^{1}H-NMR spectrum. The ^{1}H-Nuclear Magnetic Resonance (NMR) spectroscopy was used to further confirm the structure of the synthesized ligand. The ^{1}H-NMR spectrum, recorded in DMSO-d_6 as the solvent, revealed distinct proton signals corresponding to the expected functional groups and molecular framework of the ligand (Fig. 4). The spectrum exhibited a singlet at $\delta = 12.85$ ppm, which is characteristic of the carboxylic acid proton (–COOH), confirming the presence of the carboxyl group. This signal is typically downfield due to the strong deshielding effect of the electronegative oxygen atoms in the carboxyl group.[42]

In the aromatic region, multiple signals were observed between $\delta = 7.20$–8.10 ppm, corresponding to the protons on the benzene rings. Specifically, the protons associated with the benzoic acid group, and the aminophenyl ring exhibited a multiple spanning from $\delta = 7.60$ to 8.10, and from 7.20 to 7.50 ppm respectively. The splitting patterns and chemical shifts of these aromatic protons are consistent with the expected electronic environment of the ligand, where the electron-withdrawing carboxyl group and the electron-donating amino group influence the chemical shifts of the aromatic protons.[43] A singlet at $\delta = 8.50$ ppm was assigned to the imine proton (–CH═N–), which is deshielded due to the presence of the double bond between the carbon and nitrogen atoms. This signal is a key indicator of the successful formation of the Schiff base linkage.[42] Additionally, a broad singlet at $\delta = 5.80$ ppm was observed, corresponding to the amino protons (–NH_2). The broad nature of this signal is typical for amino protons, which often exchange with deuterium in the solvent, leading to peak broadening.[43]

The integration of the proton signals matched the expected stoichiometry of the ligand, further confirming its molecular structure (Fig. 5). The nonappearance of extraneous signals in the spectrum validated the high purity of the synthesized compound. The ^{1}H-NMR data, combined with the mass spectrometry results, provide strong evidence for the successful synthesis of the ligand and the integrity of its functional groups, which are critical for its adsorption capabilities.

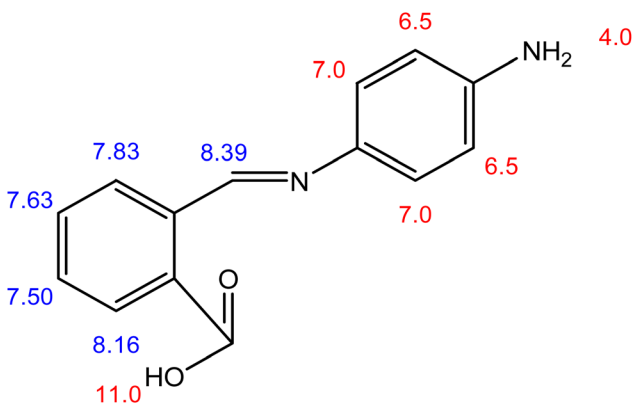

Fig. 5 Integration of proton signals confirming the ligand's stoichiometry.

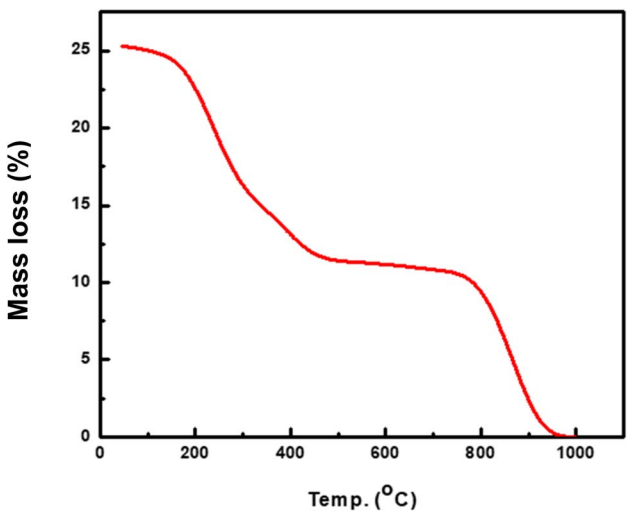

Fig. 6 The TGA curve of the prepared ligand.

Open Access Article. Published on 27 June 2025. Downloaded on 2/9/2026 7:51:31 PM.
This article is licensed under a Creative Commons Attribution-NonCommercial 3.0 Unported Licence.

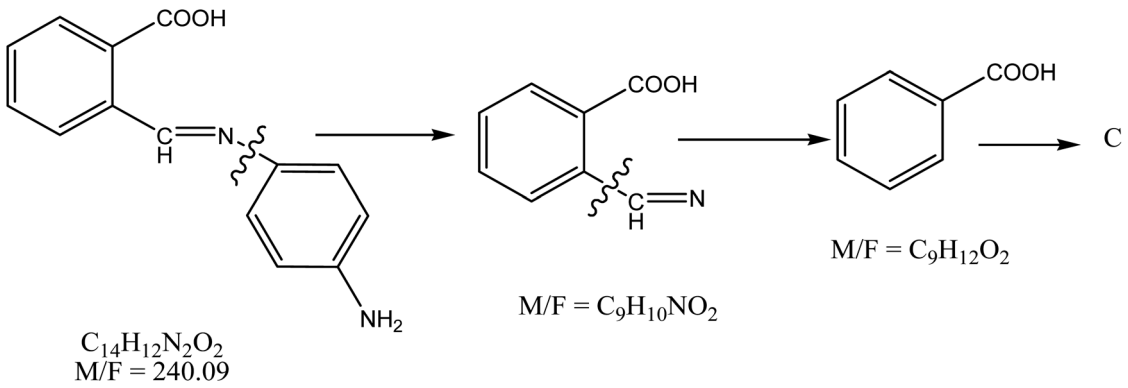

Fig. 7 The expected thermal decomposition mechanism for ligand (1).

3.1.5. Thermogravimetric analysis (TGA). Thermogravimetric analysis (TGA) was used to assess the thermal stability of the synthesized ligand. As shown in Fig. 6 the ligand remains stable up to approximately 237 °C, which corresponds to its melting point. This thermal resilience indicates the material is suitable for environmental applications under standard and moderately elevated temperatures.[23,24] Beyond this point, the ligand undergoes gradual decomposition, ultimately forming a carbonaceous residue. The mass loss observed is attributed to the breakdown of key functional groups such as amino (–NH_2), carboxyl (–COOH), and imine (–C═N), which are known to degrade at elevated temperatures. The proposed thermal decomposition mechanism (Fig. 7) reflects a stepwise loss of these functional groups, consistent with the ligand's chemical structure. This thermal profile confirms that the ligand possesses sufficient thermal robustness for practical use in water treatment applications.[42,43]

3.1.6. SEM-EDX analysis. SEM image of the ligand prior to adsorption displayed a consistent and porous surface structure, which is beneficial for adsorption owing to its extensive surface area. EDX analysis confirmed that carbon, nitrogen, and oxygen were the primary elements present, with no heavy metals detected, indicating the ligand's purity prior to adsorption experiments (Fig. 8-I). After adsorption process, the SEM images showed a rougher and more textured surface, suggesting the deposition of metal ions onto the ligand. EDX analysis post-adsorption confirmed the presence of Pb and Cd peaks, providing direct evidence of the ligand's ability to adsorb these metals (Fig. 8-II). The reduction in the relative intensities of carbon, and oxygen signals further supports the metal ions/ligand interaction.[23,24] The porous nature of the ligand, combined with the existence of –NH_2 and –COOH groups, enables efficient adsorption *via* mechanisms like chelation, electrostatic interactions, and hydrogen bonding.[42,43] The changes in surface morphology and the appearance of Pb and Cd in the EDX spectrum highlight the ligand's selectivity and capacity for heavy metal removal.

3.1.7. DLS and zeta potential analysis. The synthesized ligand was analyzed using zeta potential and dynamic light scattering (DLS) measurements, with the findings summarized in Table 1. The findings deduced that the sorbent particles exhibit an average hydrodynamic diameter of 321.6 nm,

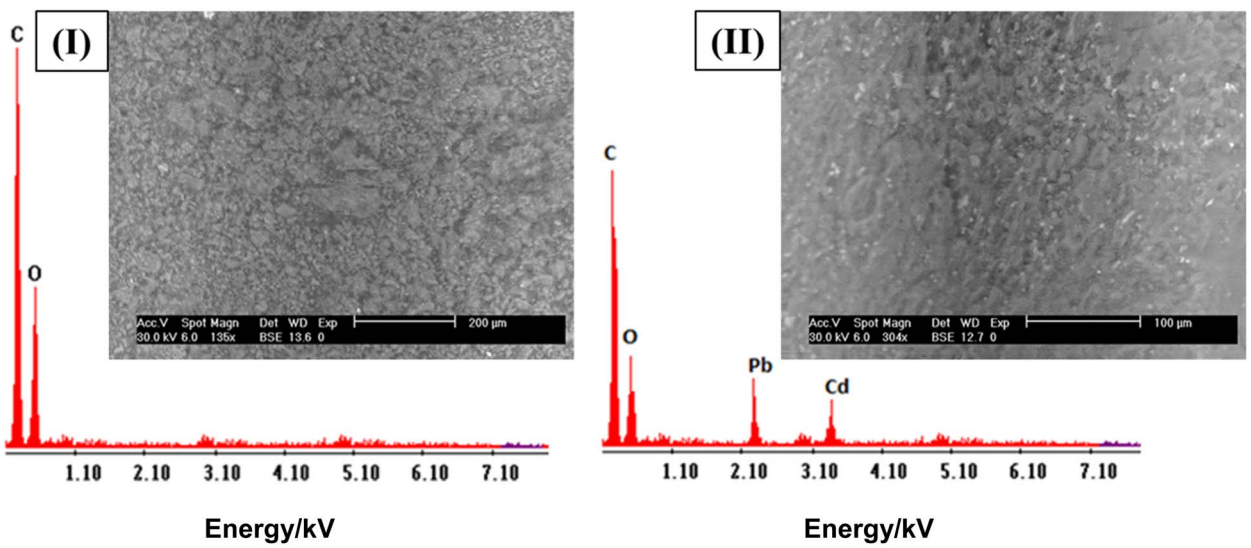

Fig. 8 SEM images and EDX spectrum of the ligand before (I) and after (II) sorption.

© 2025 The Author(s). Published by the Royal Society of Chemistry

Open Access Article. Published on 27 June 2025. Downloaded on 2/9/2026 7:51:31 PM. This article is licensed under a Creative Commons Attribution-NonCommercial 3.0 Unported Licence.

Table 1 DLS and zeta potential values of the prepared ligand

DLS analysis, nm	Zeta potential, mV
321.6	−21.4

positioning them within the nanoscale range. This nanoscale dimension enhances adsorption efficiency by maximizing the surface area relative/volume, which in turn boosts the availability of active sites for interaction with the target ions.[23,24] As a result, the material's overall adsorption capacity is significantly improved. The zeta potential measurement of −21.4 mV indicates a negatively charged surface, likely attributed to the existence of the carboxyl and amino active sites, which can undergo deprotonation in aqueous environments. This negative surface charge facilitates the adsorption of positively charged metallic pollutants through electrostatic interaction mechanism.[23,24] Additionally, the observed zeta potential value suggests moderate colloidal stability, which is essential for maintaining the sorbent's dispersion in aqueous solutions. This stability ensures effective interaction with metal ions and consistent adsorption performance throughout the process.

3.2. Batch investigation

Batch examination of the Cd(II) and Pb(II) ions uptake using the 2-((*E*)-(4-aminophenylimino)methyl)benzoic acid provides critical insights into the effects of key operational variables—solution pH, temperature, metal ion original concentration, shaking time, ligand dose, and the presence of competing ions—on the adsorption capacity. These variables were systematically studied to understand their influence on the adsorption process and to identify optimal conditions for maximum metal ion removal. The results, summarized in Fig. 9, reveal that the adsorption capacity (q_t) is highly sensitive to these variables, with each factor playing a distinct role in shaping the adsorption behavior.

Solution pH emerged as one of the most influential factors, significantly affecting the adsorption capacity, primarily due to its effect on the metal ion species in the solution and ligand surface charge.[25,44–46] The sorption capacity for both cadmium(II) and lead(II) increased with rising pH, reaching maximum values of 51.9 and 61.7 mg g^{-1} for cd(II) and Pb(II) respectively at pH 6 (Fig. 9-I). However, prolong pH 6.0, the adsorption capacity declined as a result of the formation of insoluble hydroxides (*i.e.* $Cd(OH)_2$ and $Pb(OH)_2$), which reduced the availability of free metal ions for adsorption.[25,44–46] The zeta potential of the ligand, measured at −21.4 mV (Table 1), provides further insight into the adsorption behavior at different pH levels. Under acidic conditions, the abundance of H^+ ions competes with cadmium(II) and lead(II) ions for binding sites on the ligand. This competition, along with the protonation of $-NH_2$ and –COOH groups, reduces their ability to interact with metal ions, thereby limiting adsorption efficiency.[25,44–46] The increment of solution pH result in a decline in the hydrogen ion concentration which permit the electrostatic interaction mechanism between the positive ions and negative sligand surface to take place during the adsorption process. However, at pH > 6.0, the predominant formation of insoluble metal hydroxides reduces the adsorption affinity, a trend consistent with the surface complexation formation (SCF) theory.[25,44–46] This behavior highlights the importance of pH optimization to achieve maximum adsorption efficiency while considering the interplay between electrostatic interactions and metal ion speciation.

The period of shaking significantly influenced the adsorption kinetics and capacity. For Cd(II), the uptake intensity enhanced from 8.0 to 52.0 mg g^{-1} for cadmium(II) and from 16.0 to 62.0 for lead(II) as the timeframe boost from 5 to 600 min (Fig. 9-II). The swift initial adsorption seen within the first 60 minutes (equilibrium state) is owned to the plentiful surface function groups on the ligand, while the slower progression toward equilibrium indicates the steady filling of the ligand site and the beginning of intraparticle diffusion.[25,44–48] The greater adsorption capacity and quicker kinetics for lead(II) related to cadmium(II) align with the characterization findings, which identified functional groups ($-NH_2$, –COOH, and –C═N) that interact more strongly with Pb(II) ions.

The ligand amount of addition was another key factor influencing the uptake tendency, whereas the boost of ligand dose result in the strong decline of the sorption affinity from 51.0 to 14.0, and from 62.0 to 16.6 mg g^{-1} for cadmium and lead ions (Fig. 9-III). This decline in adsorption capacity can be attributed to several reasons: (1) particle aggregation at higher doses, which decreases the available surface area; (2) excessive active sites compared to the low metal ion concentration, leading to underutilization of the sorbent's adsorption capacity.[25,45–47] Furthermore, distribution coefficient (K_d) values, calculated from experimental data, showed significant variations with changing sorbent doses (Fig. S1†). This indicates the strong complexation of cadmium(II) and lead(II) ions with the functional groups on the ligand surface.[25,45–47] This behavior underscores the importance of optimizing the ligand dosage to achieve efficient metal ion removal without excessive use of the ligand material.

The original metal ions concentration significantly influenced the adsorption capacity. The uptake intensity enhanced from 13.0 to 61.8, and from 14.6 to 76.4 mg g^{-1} for cadmium(II) and lead(II) original concentration varied from 20 to 300 mg L^{-1} (Fig. 9-IV). This pattern highlights the driving force created by higher metal ion concentrations, which enhances the probability of interactions between cadmium(II) and lead(II) and ligand function groups.[25,44–48] The consistently higher ligand uptake affinity towards lead(II) than cadmium(II) across all concentrations further emphasizes the ligand's stronger tendency for lead(II), as corroborated by the characterization data.

The impact of temperature on adsorption capacity indicated that the process is exothermic, as the capacity declined with rising temperatures. For cadmium(II), the capacity dropped from 61.8 to 46.0 mg g^{-1} as the temperature rose from 25 to 55 °C, while for Pb(II), it decreased from 51.8 to 39.0 mg g^{-1} over the same temperature range (Fig. 9-V). This trend suggests that the uptake system is exothermic and primarily driven by

Open Access Article. Published on 27 June 2025. Downloaded on 2/9/2026 7:51:31 PM.
This article is licensed under a Creative Commons Attribution-NonCommercial 3.0 Unported Licence.

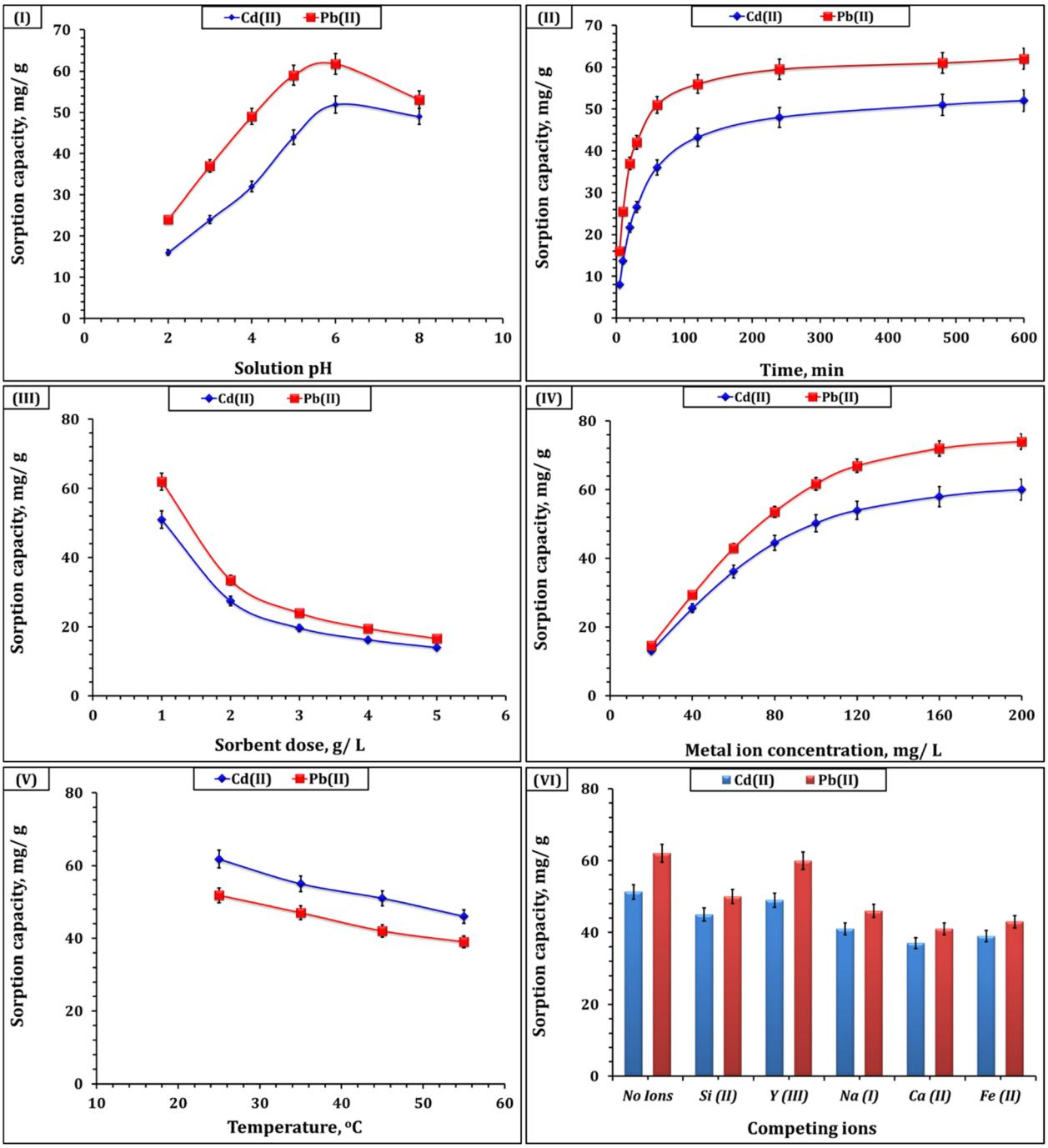

Fig. 9 Sorption tendency of lead(II), and cadmium(II) from synthetic aqueous solutions as a function of (I) solution pH (ligand dosage: 1.0 g L^{-1}; original concentration: 100 mg L^{-1}; room temperature; and time: 240 min), (II) shaking time (room temperature; ligand dosage of 1.0 g L^{-1}; original concentration of 100 mg L^{-1}; pH 5.9), (III) ligand dosage (pH 5.9; time of 240 min; original concentration: 100 mg L^{-1}; and room temperature), (IV) original concentration (time: 240 min; room temperature; pH 5.9; and ligand dosage: 1.0 g L^{-1}), (V) temperature (pH 5.9; time of 240 min; original concentration: 100 mg L^{-1}; ligand dosage: 1.0 g L^{-1}), and (VI) interfering ions (room temperature; time of 240 min; original concentration of 100 mg L^{-1}; pH 5.9; and ligand dosage: 1.0 g L^{-1}).

chemisorption. The capacity decline at higher temperatures is due to the weakening of the binding between the ligand and the target ions, as well as the increased mobility of lead(II) and cadmium(II) in the solution.[45–48]

The effect of competing ions on the adsorption efficiency was investigated to evaluate the ligand's selectivity under more realistic water conditions. In this study, competing ions—Si(II), Y(III), Na(I), Ca(II), and Fe(II)—were introduced at a concentration of 100 mg L^{-1}, chosen to reflect representative levels commonly encountered in industrial and municipal wastewater. As shown in Fig. 9-VI, the sorption capacity of the ligand for Cd(II) and Pb(II) in the absence of competing ions was

© 2025 The Author(s). Published by the Royal Society of Chemistry

Open Access Article. Published on 27 June 2025. Downloaded on 2/9/2026 7:51:31 PM. This article is licensed under a Creative Commons Attribution-NonCommercial 3.0 Unported Licence.

51.3 mg g^{-1} and 62.1 mg g^{-1}, respectively. Upon introducing competing ions, a noticeable decrease in adsorption capacity was observed, particularly in the presence of Ca(II) and Fe(II), which showed stronger interference. This reduction can be attributed to competition for available binding sites and, in some cases, the formation of aqueous metal complexes that limit free ion availability.

The batch investigation highlights the effectiveness of the synthesized ligand for the capture of metallic pollutants, with the adsorption capacity influenced by a combination of temperature, original ion concentration, ligand dose, shaking time, solution pH, and the presence of competing ions. The same performance was also deduced for cadmium(II) and lead(II) ions adsorption from aqueous solution using iron nanoparticles embedded within cellulose nanofibrils,[44] Magnetic nanoparticles coated with chitosan nanoparticles, cross-linked with succinic anhydride, and cross-linked with crotonaldehyde,[25] Spirodela polyrhiza biomass,[45] oxidized multiwalled carbon nanotubes (oxMWCNTs),[46] biochar decorated with sulfide-iron(BC-Fe-S),[47] and cotton fabric functionalized with nanostructured molybdenum disulphide (MoS_2).[48] These findings provide important understandings into the optimization of process conditions and underscore the potential of this ligand for practical applications in wastewater treatment and environmental remediation, particularly in scenarios involving complex aqueous matrices.

3.3. Sorption kinetic investigation

The kinetics of lead(II) and cadmium(II) adsorption using the synthesized ligand, 2-(*E*)-(4-aminophenylimino)methylbenzoic acid, were extensively studied to comprehend the rate and mechanism of the capture process. Conventional kinetic models included Morris–Weber, Elovich, pseudo-second-order (PSO), and pseudo-first-order (PFO) models were employed for the assessment of the gained experimental data. These models together offer insights into the adsorption mechanism, indicating a multi-step process that includes chemisorption, surface heterogeneity, and intraparticle diffusion.[32,33] The kinetic curves for lead(II) and cadmium(II) capture are illustrated in Fig. 10, however the variables of the applied kinetic equations are summarized in Table 2.

The PFO model assumes that the rate of adsorption is proportional to the number of unoccupied sites. While it gave a good fit with R^2 values of 0.98 for both metal ions, it underestimated the actual equilibrium capacities. For Cd(II), the calculated capacity was 48.6 mg g^{-1} ($k_1 = 0.026$ min^{-1}), and for Pb(II), it was 59.5 mg g^{-1} ($k_1 = 0.049$ min^{-1}). The relatively high average relative error (ARE) values—8.6% for Cd(II) and 6.1% for Pb(II)—suggest that the model does not fully capture the true kinetics. In contrast, In contrast, the PSO model provided a much closer fit to the experimental data, with R^2 values of 0.99 for both ions and significantly lower ARE values (1.21% for

Table 2 The values of the parameters used in the applied kinetics model

	Cd(II)	Pb(II)
Pseudo first-order model		
q_1 (mg g^{-1})	48.6	59.5
k_1 (min^{-1})	0.026	0.049
R^2	0.98	0.98
ARE	8.65	6.14
Pseudo second-order model		
q_2 (mg g^{-1})	54.3	63.0
k_2 (min^{-1})	0.0006	0.0011
h (mol g^{-1} h^{-1})	1.8	4.3
$t_{1/2}$ (h)	30.7	14.6
R^2	1.00	1.00
ARE	1.21	0.5
Elovich model		
α (mg g^{-1} min^{-1})	0.10	0.09
β (g mg^{-1})	4.07	11.39
R^2	0.97	0.92
ARE	10.3	8.8

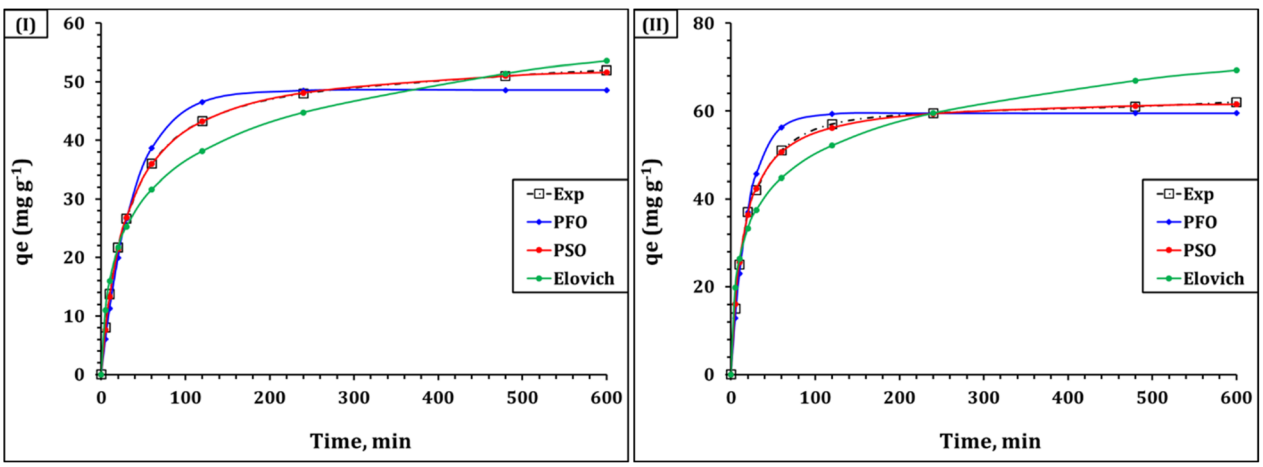

Fig. 10 Kinetic curves for Cd(II) and Pb(II) adsorption from synthetic aqueous solutions (solution pH 6.01; ligand dose of 1.0 g L^{-1}; original concentration of 100 mg L^{-1}; temperature of 25 ± 1 °C).

Open Access Article. Published on 27 June 2025. Downloaded on 2/9/2026 7:51:31 PM. This article is licensed under a Creative Commons Attribution-NonCommercial 3.0 Unported Licence.

Cd(II) and 0.5% for Pb(II)). The calculated equilibrium adsorption capacities (q_2) were 54.3 mg g^{-1} for Cd(II) and 63.0 mg g^{-1} for Pb(II), which closely matched the actual values. The corresponding rate constants (k_2) were 0.0006 min^{-1} for Cd(II) and 0.0011 min^{-1} for Pb(II). The higher initial sorption rate (h) for Pb(II) (4.3 mol g^{-1} h^{-1}) compared to Cd(II) (1.8 mol g^{-1} h^{-1}), along with the shorter half-equilibrium time (14.6 h *vs.* 30.7 h), confirms the ligand's stronger affinity for Pb(II). These findings indicate that chemisorption is the dominant mechanism for both ions, likely involving valence forces through sharing or exchange of electrons between the ligand and metal ions.[44,46,47]

The Elovich model, which describes adsorption on energetically heterogeneous surfaces, also fit the data well, supporting the involvement of diverse surface sites in the process. The initial adsorption rate (α) was found to be 0.10 mg g^{-1} min^{-1} for Cd(II) and 0.09 mg g^{-1} min^{-1} for Pb(II), with desorption constants (β) of 4.07 g mg^{-1} and 11.39 g mg^{-1}, respectively. These values support the presence of a non-uniform surface and a gradual increase in activation energy during adsorption, consistent with surface heterogeneity.[37,38] The Morris–Weber model was applied to further investigate the role of intraparticle diffusion in the uptake system.[32,33] The model formula (Table S1†) was used to illustrate the variation of the sorption affinity (q_t) with time 0.5 (Fig. 11), and the explored model terms are displayed in Table S2.† The anticipated data explored that the rate constant (k_i) was 2.23 and 1.68 mg g^{-1} min 0.5 for lead(II) and cadmium(II), with boundary layer constants (C) of 12.0 and 14.2, respectively. The high R^2 values (0.96 for both Cd(II) and Pb(II)) reflects the contribution of the intraparticle diffusion mechanism in the capture process.[44,46,47] However, the non-zero values of C indicate that boundary layer diffusion also contributes to the overall adsorption mechanism, particularly in the initial stages of the process.[44,46,47]

The integrated analysis of the kinetic models indicates that the sorption of lead(II) and cadmium(II) onto the synthesized sorbent involves multiple steps. The initial rapid adsorption is primarily driven by chemisorption and boundary layer diffusion, as indicated by the PSO model and the non-zero C values in the W–M model. This is followed by gradual intraparticle diffusion into the porous structure of the ligand, as described by the Morris–Weber model. The same kinetic performance were illuminated for cadmium(II) and lead(II) adsorption from aqueous solution using iron nanoparticles embedded within cellulose nanofibrils,[44] magnetic nanoparticles coated with chitosan nanoparticles, cross-linked with succinic anhydride, and cross-linked with crotonaldehyde,[25] Spirodela polyrhiza biomass,[45] oxidized multiwalled carbon nanotubes (oxMWCNTs),[46] biochar decorated with sulfide-iron(BC-Fe-S).[47]

The IR and ^{1}H-NMR spectrums (Fig. 3 and 4 respectively) confirmed the existence of functional groups (–COOH, $–NH_2$, and –C=N) that are essential for chemisorption, as indicated by the PSO model. The mass spectrometry data (Fig. 2) validated the molecular integrity of the ligand, ensuring that the functional groups remain intact and available for metal ion coordination. The porous structure of the ligand (Fig. 5), as suggested by the Morris–Weber model, provides a large surface area and multiple active sites for adsorption, enhancing the overall efficiency of the process. The kinetic investigation highlights the effectiveness of the synthesized ligand for heavy metal removal, with potential applications in wastewater treatment and environmental remediation. The dominance of chemisorption, supported by the PSO model and characterization results, underscores the critical role of active sites in the sorption process. The contributions of intraparticle diffusion and surface heterogeneity, as revealed by the Morris–Weber and Elovich models, further enhance the ligand's performance by providing multiple pathways for metal ion uptake.

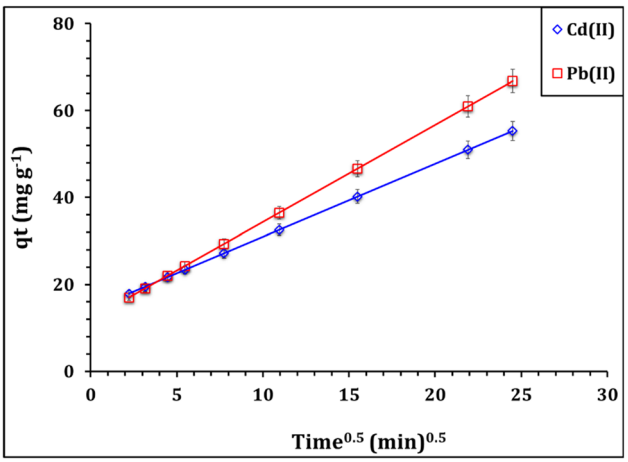

Fig. 11 Weber–Morris model illustrating intraparticle diffusion for Pb(II) and Cd(II) adsorption from synthetic solutions (solution pH 6.01; ligand dose of 1.0 g L^{-1}; original concentration of 100 mg L^{-1}; temperature of 25 ± 1 °C).

3.4. Sorption isotherms

The adsorption isotherms for lead(II) and cadmium(II) ions using the synthesized ligand were conducted to elucidate the equilibrium behavior besides the adsorption capacity under varying initial metal ion concentrations. The isotherm profiles, depicted in Fig. 12, demonstrate the direct proportional relationship between the sorption capacity and ions original concentration, eventually reaching a plateau at higher concentrations. This saturation behavior indicates that the available function groups on the ligand surface bonded with the target ions, limiting further adsorption.[34,35] To gain deeper understandings into the surface properties and uptake mechanism, the revealed results were analyzed using four commonly applied isotherm models: Temkin, Sips, Freundlich, and Langmuir. These models together offer a thorough understanding of the adsorption process, encompassing surface homogeneity, heterogeneity, and the characteristics of adsorbate–ligand interactions.[34,35] The explored isotherm parameters were displayed in Table 3.

The Langmuir isotherm model, which suggests that monolayer adsorption happens on a uniform surface with a limited number of identical sites, showed a strong correlation with the experimental data. For Cd(II), the maximum adsorption capacity (q_m) was 71.0 mg g^{-1}, while Langmuir constant (k_i) was 0.044 L

© 2025 The Author(s). Published by the Royal Society of Chemistry

Open Access Article. Published on 27 June 2025. Downloaded on 2/9/2026 7:51:31 PM.
This article is licensed under a Creative Commons Attribution-NonCommercial 3.0 Unported Licence.

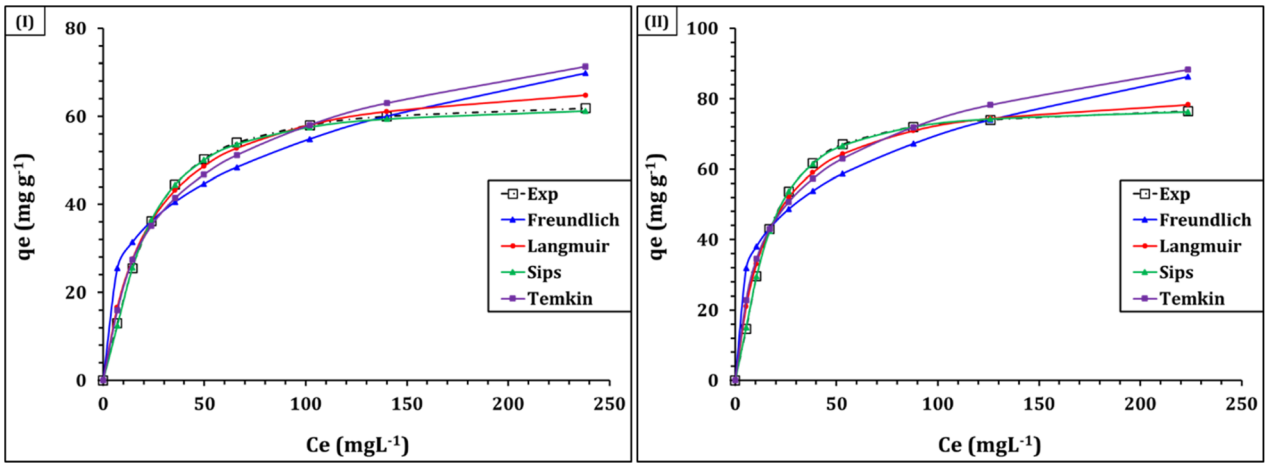

Fig. 12 Isotherm profile for the sorption of lead(II) and cadmium(II) ions from synthetic solution (time is 240 min; ligand dose of 1.0 g L^{-1}; pH 5.9; temperature of 25 ± 1 °C).

Table 3 Parameters of the applied isotherm models

	Cd(II)	Pb(II)
Langmuir model		
q_m (mg g^{-1})	71.0	84.0
k_L (L mg^{-1})	0.044	0.062
R^2	0.99	0.99
ARE	5.7	7.9
Freundlich model		
$1/n_F$	0.3	0.3
k_F (mg g^{-1}) (mg L^{-1})	14.7	20.3
R^2	0.86	0.84
ARE	18.7	22.4
Temkin model		
b_T (J mol^{-1})	157.8	140.8
A_T (L g^{-1})	0.4	0.7
R^2	0.95	0.93
ARE	8.0	12.6
Sips model		
q_s (mg g^{-1})	63.0	78.0
k_s (L mg^{-1})	0.053	0.067
m_s	1.40	1.40
R^2	0.99	0.99
ARE	0.9	0.6

mg^{-1}, and a correlation coefficient (R^2) of 0.99. For Pb(II), the values were 84.0 mg g^{-1} for q_m, 0.062 L mg^{-1} for k_i, and an R^2 of 0.99. The high R^2 values and low average relative error (ARE) values (7.9 and 5.7 for lead(II) and cadmium(II) respectively) demonstrate that the Langmuir model effectively characterizes the adsorption process, indicating that the ligand surface is relatively uniform and that adsorption occurs primarily through monolayer coverage.[34,35,44] This is consistent with the existence ligand surface function groups (–NH_2, –COOH, and –C═N), which provide well-defined sites for metal ion binding, as confirmed by IR, ^{1}H-NMR, and mass spectrometry characterization results (Fig. 3, 4, and 2 respectively). Similar isotherm performance (*i.e.* homogeneous and monolayer coverage adsorption process) were illuminated for cadmium(II) and lead(II) adsorption from aqueous solution onto iron nanoparticles embedded within cellulose nanofibrils,[44] oxidized multiwalled carbon nanotubes (oxMWCNTs),[46] Biochar decorated with sulfide-iron(BC-Fe-S),[47] ZnO nanoparticles loaded onto biochar derived from cassava root husk (CRHB-ZnO3),[34] and Bauhinia purpurea powder.[35]

It is worth noted that, the nature of the uptake system can be evaluated using the dimensionless equilibrium variable (R_l), calculated as $R_l = 1/(1 + K_l C_0)$. Based on its value, sorption behavior is classified as irreversible ($R_l = 0$), linear ($R_l = 1$), unfavorable ($R_l > 1$), or favorable ($0 < R_l < 1$).[34,35] The R_l values obtained, as shown in Fig. S2,† indicate that the sorption process is favorable, with Cd(II) displaying R_l values ranging from 0.07 to 0.53 and Pb(II) showing values between 0.05 and 0.44 across all initial concentrations tested.

The Freundlich isotherm model, which describes the heterogeneity of the sorbent surface, also provided a reasonable fit to the experimental data. For Cd(II), the Freundlich constant (K_f) was 14.7 (mg g^{-1})(L mg^{-1}), with an intensity parameter ($1/n$) of 0.3 and an R^2 of 0.86. For Pb(II), the values were 20.3 (mg g^{-1})(L mg^{-1}) for K_f, 0.3 for $1/n$, and an R^2 of 0.84. The Freundlich model's fit suggests that the ligand surface is heterogeneous, with multiple active sites contributing to the adsorption process.[34,35,44] This aligns with the findings from the kinetic investigation, where the Elovich and Morris–Weber models also indicated surface heterogeneity. The parameter $1/n$ is commonly used to assess the sorption favorability. A sorption process is considered favorable when $0 < 1/n < 1$, while a value of $1/n = 1$ indicates an irreversible process, and if $1/n$ exceeds 1, the adsorption is classified as unfavorable.[34,35] According to Table 3, the uptake of lead(II) and cadmium(II) is favorable, as reflected by $1/n$ values of 0.1, which is reliable with the outcomes from the Langmuir dimensionless parameter (R_l).

The Temkin isotherm model which takes into account the interactions between the adsorbate and the ligand, provided

Open Access Article. Published on 27 June 2025. Downloaded on 2/9/2026 7:51:31 PM. This article is licensed under a Creative Commons Attribution-NonCommercial 3.0 Unported Licence.

additional insights into the adsorption mechanism.[35,46] For Cd(II), the Temkin constant (b_t) was 157.8 J mol^{-1}, with an equilibrium binding constant (A_t) of 0.4 L g^{-1} and an R^2 of 0.95. For Pb(II), the values were 140.8 J mol^{-1} for b_t, 0.7 L g^{-1} for A_t, and an R^2 of 0.93. The parameters of the Temkin model suggest an exothermic and physisorption process whereas the sign and magnitude of the b_t values for both metal ions are positive and <8 kJ mol^{-1}.[35,46] In addition, the A_t values for Pb(II) > Cd(II) confirming the higher affinity of the applied ligand that towards Pb(II) ions, which aligns with the finding from Langmuir model.

Lastly, the Sips isotherm model, which integrates aspects of both the Freundlich and Langmuir models, was employed for addressing both monolayer adsorption and surface heterogeneity.[31,36] For Cd(II), 63.0 mg g^{-1} was the Sips maximum uptake capacity (q_s), while Sips constant (K_s) was 0.053 L mg^{-1} and an R^2 of 0.99. For Pb(II), the values were 78.0 mg g^{-1} for q_s, 0.067 L mg^{-1} for K_s, and an R^2 of 0.99. The Sips model's excellent fit to the anticipated results, along with low ARE values (0.6 and 0.9 for lead(II) and cadmium(II) respectively), further supports the hypothesis that the uptake system involves both monolayer coverage and heterogeneous surface interactions. The parameter m_s, which represents the heterogeneity factor, was 1.40 for both lead(II) and cadmium(II), indicating a moderate level of surface heterogeneity.[31,36] This finding is consistent with the Freundlich model's suggestion of surface heterogeneity and aligns with the kinetic results, which indicated a multi-step adsorption process involving chemisorption and intraparticle diffusion.

The comprehensive analysis of isotherm models indicates that lead(II) and cadmium(II) ions capture by the synthesized ligand involves multiple concurrent mechanisms. While the Langmuir model suggests predominantly homogeneous surface interactions with discrete, equivalent binding sites, the Freundlich and Sips models reveal significant surface heterogeneity with diverse active sites participating in adsorption. The Temkin model further demonstrates the importance of physisorption mechanisms, particularly electrostatic interactions between the ligand and metal ions. These theoretical findings align with experimental characterization data, which confirmed the occurrence of key efficient groups (–COOH, –NH_2, and –C═N) facilitating chemisorption, a negatively charged surface enabling electrostatic interactions, and a porous structure providing extensive surface area with multiple binding sites. The Weber–Morris kinetic model corroborates this multi-mechanism adsorption process, suggesting a complex interplay between different binding modes.

The synthesized ligand, enhanced with –NH_2, –COOH, and –C═N groups, exhibits a notably stronger tendency for lead(II) ions than cadmium(II) ions. This distinction can be explained by a mix of physicochemical factors and principles of coordination chemistry. Several parameters influence the adsorption affinity of metal ions, including ionic radius, hydrolysis constant, electronegativity, and hydration energy.[30,39] For instance, titanium phosphate ion-exchangers show a preference for Pb^{2+} over other ions, attributed to the ion's smaller hydrated radius, which facilitates better interaction with the sorbent.[39] Similarly, electronegativity governs metal ion adsorption by enhancing polarization and coordination, as seen in zeolite selectivity ($Pb^{2+} > Zn^{2+} > Cd^{2+} > Cu^{2+}$), where ionic steric effects also play a role.[49] The adsorption capacities of Cu^{2+}, Cd^{2+}, Ni^{2+}, and Zn^{2+} ions onto carbon-based sorbents were correlated with electronegativity theory, indicating that ions with higher electronegativity were more readily adsorbed. Variations in hydration energy also influence the adsorption process, affecting the interaction with carboxylic functional groups on ligands.[50] Furthermore, Chu *et al.* (2018) reported that the ion hydrolysis ability of metals significantly influences adsorption, with variations in metal ion hydrolysis constants affecting the adsorption process. Specifically, changes in ionization potential and hydrolysis promote adsorption, while certain properties inhibit it.[51]

A key factor in the superior adsorption of Pb(II) is its larger ionic radius (1.19 Å) compared to Cd(II) (0.95 Å), which facilitates more effective coordination with the ligand's functional groups.[52,53] Additionally, Pb(II) exhibits a higher electronegativity (2.33 on the Pauling scale) than Cd(II) (1.69), leading to stronger electrostatic and covalent interactions with the ligand surface.[54] Charge density also plays a crucial role in adsorption behavior. Pb(II) has a lower charge density (32 C mm^{-3}) than Cd(II) (59 C mm^{-3}), reducing electrostatic repulsion with the electron-rich functional groups (–NH_2, –COOH, and –C═N).[55] This lower repulsion allows Pb(II) to form more stable complexes with the ligand. In contrast, the higher charge density of Cd(II) results in greater repulsion, limiting its adsorption efficiency. Moreover, Cd(II) has a significantly higher hydration energy (−1807 kJ mol^{-1}) compared to Pb(II) (−1481 kJ mol^{-1}), meaning Cd(II) ions are more strongly solvated in aqueous solutions.[54] This strong solvation further reduces their availability for adsorption. From a coordination chemistry perspective, Pb(II) typically forms a higher coordination number (7.5) than Cd(II) (6.25), enabling stronger interactions with multiple sorbent surface function groups.[56] Additionally, lead(II) is considered as a borderline Lewis acid (0.266), whereas Cd(II) is a softer Lewis acid (0.320).[57] Given that the ligand's functional groups (–NH_2, –COOH, and –C═N) are intermediate or soft bases, they exhibit a higher tendency for borderline acids such as lead(II) due to more favorable orbital overlap and bonding interactions. Although Cd(II) can also form stable complexes with soft bases, its higher solvation energy, charge density, and lower electronegativity reduce its competitive adsorption in this system.

These outcomes emphasize the potential of the synthesized ligand for selective heavy metal removal, particularly in wastewater treatment and environmental remediation applications where Pb(II) contamination is a concern. The material's high adsorption capacity and strong interactions with Pb(II) suggest its effectiveness for targeted heavy metal removal. The present work illuminates valuable insights for the design and optimization of ligands, highlighting the critical role of factors such as ionic radius, electronegativity, charge density, hydration energy, coordination chemistry, and HSAB theory in governing adsorption behavior.

Table 4 elucidate the uptake affinity of the prepared ligand in regards to other materials from the literature. The findings

© 2025 The Author(s). Published by the Royal Society of Chemistry

Open Access Article. Published on 27 June 2025. Downloaded on 2/9/2026 7:51:31 PM. This article is licensed under a Creative Commons Attribution-NonCommercial 3.0 Unported Licence.

Table 4 Comparison of adsorption capacities of various sorbents for Pb(II) and Cd(II) removal from aqueous solutions

Name	Time, min	pH	Initial conc., mg L^{-1}	Temp., oC	Q_e, mg g^{-1}	R
Pb(II)						
Cellulose nanofibrils impregnated with iron nanoparticles	150	5.0	5–500	40	89.08	44
Spirodela polyrhiza biomass	120	6.0	100–160	25	36.0	45
Oxidized multiwalled carbon nanotubes	1440	5.0	0.5–5.0	25	10.5	46
Cassava root husk-derived biochar	60	6.0	20–100	25	34.47	34
ZnO nanoparticles loaded onto biochar derived from cassava root husk					44.27	
Bauhinia purpurea powder	1440	4.5	2–100	45	23.61	35
Magnetic bauhinia purpurea powder					20.01	
Polymer-modified magnetic nanoparticles	45	5.5	20–450	25	166.1	58
Egyptian Na-activated bentonite	60	3.8	5–20	25	5.43	59
2-((*E*)-(4-aminophenylimino)methyl) benzoic acid	240	6.0	20–300	25	84.0	PW
Cd(II)						
Cellulose nanofibrils impregnated with iron nanoparticles	150	5.0	5–500	40	14.48	44
Spirodela polyrhiza biomass	120	4.0	10–40	25	137	45
Oxidized multiwalled carbon nanotubes	1440	5.0	0.5–5.0	25	23.4	46
Cassava root husk-derived biochar	60	6.0	20–100	25	32.33	34
ZnO nanoparticles loaded onto biochar derived from cassava root husk					42.05	
Bauhinia purpurea powder	1440	5.0	2–100	25	11.13	35
Magnetic bauhinia purpurea powder					4.76	
Polymer-modified magnetic nanoparticles	45	5.5	20–450	25	29.6	58
Egyptian Na-activated bentonite	60	3.8	5–20	25	3.145	59
2-((*E*)-(4-aminophenylimino)methyl) benzoic acid	240	6.0	20–300	25	71.0	PW

illuminate that the synthesized ligand, 2-((*E*)-(4-aminophenylimino)methyl) benzoic acid, displays outstanding uptake affinity of 84.0 and 71.0 mg g^{-1} for cadmium and lead ions respectively, exceeding those of sorbents like Bauhinia purpurea powder, iron nanoparticles embedded within cellulose nanofibrils, and ZnO-loaded biochar. This high efficiency is attributed to the ligand's unique molecular structure, which includes amino ($-NH_2$), carboxyl (–COOH), and imine (–C=N) groups that facilitate strong coordination, electrostatic interactions, and chelation with metal ions. In contrast, materials like polymer-modified magnetic nanoparticles and oxidized multiwalled carbon nanotubes exhibit moderate adsorption capacities, while biochar-based sorbents show comparatively lower performance. Overall, the synthesized ligand stands out as a highly effective ligand for the capture of cadmium and lead ions from aqueous solutions. Its superior uptake capacity, combined with its structural and functional properties, makes it a highly suitable option for environmental remediation.

3.5. Thermodynamic investigation

Thermodynamic investigation of lead(II) and cadmium(II) capture onto the prepared ligand offers essential insights into the spontaneity, nature, and feasibility of the uptake system.[60,61] The thermodynamic parameters, (*i.e.* the standard entropy change ($\Delta S°$), standard enthalpy change ($\Delta H°$), and standard Gibbs free energy change ($\Delta G°$) were detected by the Van't Hoff plot (Fig. 13) and equations detailed in Table S1,† with results summarized in Table 5. The negative $\Delta G°$ values observed across the temperature range (20–50 °C) for both target ions demonstrate the spontaneous nature of the uptake system.[25,44,45,47] Notably, the decreasing $\Delta G°$ values with rising temperature indicate enhanced process spontaneity at higher temperatures, particularly for Pb(II). These findings align with

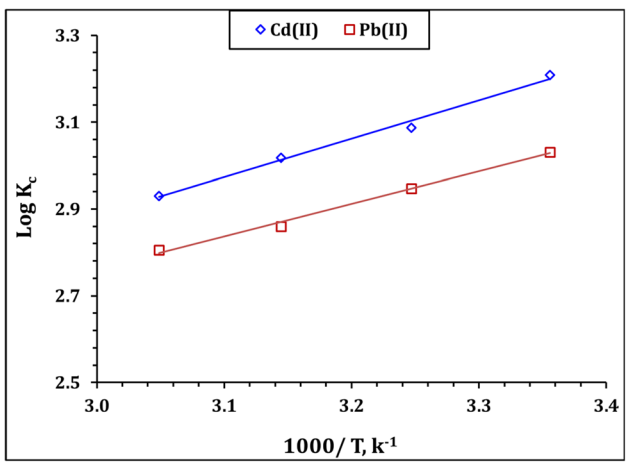

Fig. 13 Thermodynamic profiles of Cd(II) and Pb(II) adsorption from synthetic aqueous solutions (initial concentration of 100 ppm; pH 5.9; ligand dose of 1.0 g L^{-1}; shaking time is 240 min).

Table 5 The values of the thermodynamic parameters

	ΔG (kJ mol^{-1})				ΔH	ΔS
	20 °C	30 °C	40 °C	50 °C	(kJ mol^{-1})	(J mol^{-1} K)
Cd(II)	−18.31	−18.21	−18.37	−18.40	−16.98	4.47
Pb(H)	−17.30	−17.38	−17.41	−17.62	−14.34	9.93

Open Access Article. Published on 27 June 2025. Downloaded on 2/9/2026 7:51:31 PM. This article is licensed under a Creative Commons Attribution-NonCommercial 3.0 Unported Licence.

the strong metal–ligand interactions evidenced by FTIR, ^{1}H-NMR, and mass spectrometry analyses.

The negative $\Delta H°$ values (−16.98 and 14.34 kJ mol^{-1} for cadmium(II) and lead(II)) respectively) reveal the exothermic nature of the adsorption process, manifesting through dual mechanisms: chemisorption and physisorption.[25,44,45,47] Kinetic model of pseudo-second-order supports the chemisorption component through ions interactions with functional groups (–NH_2, –COOH, and –C=N), while the Temkin isotherm and zeta potential measurements confirm the physisorption mechanism *via* electrostatic interactions. This dual-mechanism interpretation explains the observed decrease in adsorption capacity at elevated temperatures (Fig. 13), as the exothermic process naturally diminishes with increasing thermal energy.

The positive $\Delta S°$ values (4.47 and 9.93 J mol^{-1} K for cadmium(II) and lead(II)) respectively) indicate the randomness boost at the liquid/solid interface through sorption.[25,44,45,47] The higher $\Delta S°$ value for Pb(II) suggests more extensive system disorder during its adsorption, likely due to its larger ionic radius and higher electronegativity enhancing interactions with the ligand's functional groups. Studies on lead(II) and cadmium(II) ion adsorption onto materials such as iron nanoparticles embedded within cellulose nanofibrils,[44] Magnetic nanoparticles coated with chitosan nanoparticles, cross-linked with succinic anhydride, and cross-linked with crotonaldehyde,[25] Spirodela polyrhiza biomass,[45] and biochar decorated with sulfide-iron(BC-Fe-S)[47] have demonstrated a spontaneous, feasible, and exothermic adsorption process.

These thermodynamic findings complement the kinetic and isotherm analyses while providing fundamental insights for optimizing heavy metal removal applications. The comprehensive understanding of the process energetics, combined with the dual-mechanism interpretation, offers valuable guidance for future ligand design and process optimization in environmental remediation contexts.

3.6. Proposed adsorption mechanisms

The capture of cadmium(II) and lead(II) from aqueous solutions using organic ligands and functionalized sorbents has been extensively studied. The mechanisms typically involve a combination of coordination bonding, electrostatic binding, and chelation.[34,35,44,47,48] Ligands containing functional groups for example amino, carboxyl, and imine exhibit high affinity for metallic pollutants owned to their aptitude for forming stable complexes through electron donation and coordination bonding.[58,62] For example, Schiff base ligands, which contain imine groups, are known for their strong chelating properties, enabling them to bind metal ions through nitrogen and oxygen donor atoms. Similarly, carboxyl groups can deprotonate in aqueous solutions to form carboxylate anions, which interact electrostatically with cations.[9–12]

Lead and cadmium ions illumination using iron nanoparticles embedded within cellulose nanofibrils occurs through exchange, electrostatic interactions, complexation, hydrogen bonding, and chelation mechanisms.[44] Biochar decorated with sulfide-iron(BC-Fe-S) binds Cd^{2+}/Pb^{2+} primarily through co-precipitation, ion exchange, chelation, and electrostatic interactions.[47] Similarly, the high adsorption capacity of MoS_2-functionalized cotton fabric for Pb, Hg, and Cd is attributed to the robust acid/base coordination between ions and surface sulfide sites.[48] Adsorption of Cr^{6+}, As^{3+}, Cd^{2+}, and Pb^{2+} onto ZnO-loaded cassava root husk biochar is mainly driven by surface precipitation and cation exchange owned to functional groups enriched with oxygen.[34] Bauhinia purpurea pods-derived magnetic and non-magnetic biosorbents remove Cd^{2+} and Pb^{2+} through hydrogen bonding, ion exchange, and chelation mechanisms.[35] Electrostatic interactions dominate the uptake of Cu(II), Pb(II), and Cd(II) onto MIL-100(Fe) and MIL-101(Cr),[62] while chelation is the primary mechanism for Pb^{2+}, Cd^{2+}, and Zn^{2+} capture using Chelating resin with hyper cross-linking and nanometer-sized particles, where amide oxygen and nitrogen atoms form stable metal complexes.[58] Additionally, Ge *et al.* reported that Cd^{2+}, Zn^{2+}, Pb^{2+}, and Cu^{2+} interact with Fe_3O_4@-APS@AA-*co*-CA ligands *via* chelation with carboxylate anions.[63]

In this study, cadmium(II) and lead(II) uptake onto the synthesized ligand, 2-((*E*)-(4-aminophenylimino)methyl) benzoic acid, involves a combination of chemical and physical mechanisms, driven by the ligand's unique structural and functional properties. The ligand's molecular structure, characterized by the presence of an amino group (–NH_2), a carboxyl group (–COOH), and an imine group (–C=N), provides multiple active sites for metal ion binding, making it highly effective for the adsorption of cadmium(II) and lead(II) from aquatic systems. The zeta potential of the ligand, measured at −21.4 mV (Table 1), confirms that the ligand possess a negative charge which enhances electrostatic binding with Cd^{2+} and Pb^{2+}. This electrostatic attraction is a key physisorption mechanism, particularly at moderate pH values where the surface charge is most pronounced.

At the same time, the chemisorption nature of the removal process, as evidenced by the PSO model, deduced that chemical interactions are the rate-limiting step. This aligns with the strong interactions between the metal ions and the ligand's functional groups. The amino group (–NH_2) has a crucial impact on the adsorption mechanism, acting as an electron donor through its lone pair of electrons. This facilitates the formation of coordination bonds with Cd^{2+} and Pb^{2+} ions, which act as Lewis acids.[48,57] The carboxyl group (–COOH) further enhances adsorption through chelation and electrostatic interactions, particularly when deprotonated to form a carboxylate anion (–COO^-).[44,63] Additionally, the imine group (–C=N), formed *via* Schiff base condensation, contributes to the adsorption process by providing another coordination site for metal ions.[9,10,58] The presence of these functional groups was confirmed by FTIR, ^{1}H-NMR, and mass spectrometry characterization (Fig. 3, 4, and 2 respectively), which revealed the ligand's structural integrity and its ability to form stable complexes with metal ions. These chemisorption mechanisms are supported by FTIR analysis for the spent ligand (Fig. 3), which shows shifts and intensity changes in the ν(NH), ν(C=O), and ν(C=N) bands after adsorption, indicating direct involvement of these functional groups in metal complexation.

© 2025 The Author(s). Published by the Royal Society of Chemistry

Open Access Article. Published on 27 June 2025. Downloaded on 2/9/2026 7:51:31 PM. This article is licensed under a Creative Commons Attribution-NonCommercial 3.0 Unported Licence.

The isotherm studies further corroborated the chemisorption mechanism, whereas the experimental data was best matched by the Langmuir and Sips models. The Langmuir model's assumption of monolayer adsorption on a uniform surface matches the ligand's well-defined active sites, while the Sips model's inclusion of surface heterogeneity reflects the ligand's ability to adsorb metal ions through multiple pathways.[34,35] The Weber–Morris kinetic model illuminated that the uptake process is controlled multiple interaction mechanisms (Fig. 10). At the beginning of the process, chemisorption mechanisms for example surface complexation, dominate the system, while physisorption mechanisms, for instance interparticular diffusion, become more significant after equilibrium is reached. The occurrence of physisorption during the elimination of cadmium(II) and lead(II) is also confirmed by thermodynamic and Temkin isotherm analyses, which indicate ΔH° values of −14.34 and −16.98 kJ mol^{-1} (Table 5) and heats of adsorption of 140.8 and 157.8 (Table 3) for lead and cadmium ions respectively. These findings suggest that physisorption, *via* weak van der Waals interactions, plays a role in the removal of metal cations.[25,44,45]

In summary, the capture mechanism of lead(II) and cadmium(II) ions onto 2-((*E*)-(4-aminophenylimino)methyl) benzoic acid is governed by a synergistic interplay of chemical and physical interactions, ensuring an efficient metal capture system. The initial chemisorption phase establishes strong and selective metal binding through coordination with functional groups, while subsequent physisorption contributions enhance adsorption capacity *via* secondary interactions. This dynamic adsorption process, shaped by the temporal evolution and spatial organization of binding mechanisms, is reinforced by comprehensive analytical techniques and theoretical models. Such an in-depth mechanistic understanding provides a robust framework for optimizing metal removal strategies, particularly in complex aqueous environments, where leveraging multiple binding modes can significantly improve adsorption efficiency, making this approach highly promising for environmental remediation applications.

3.7. Desorption and recyclinginvestigations

The desorption investigation of lead(II) and cadmium(II) from the loaded ligand provides critical insights into the regeneration potential and recycling of the synthesized ligand, which is essential for its practical application in wastewater treatment. Desorption efficiency was evaluated using sulfuric (H_2SO_4), hydrochloric (HCl), and nitric (HNO_3) acids at 0.5 M and 1.0 M concentrations. The results in Fig. S3† show that HNO_3 exhibited the highest desorption efficiency, with 0.5 M achieving 84.0% (Pb^{2+}) and 83.0% (Cd^{2+}), while 1.0 M reached 97.0% and 95.0%, respectively. In contrast, H_2SO_4 and HCl showed lower efficiencies, with 1.0 M H_2SO_4 achieving 74.0% (Pb^{2+}) and 70.0% (Cd^{2+}), and 1.0 M HCl reaching 70.0% (Pb^{2+}) and 65.0% (Cd^{2+}). These findings confirm HNO_3 as the most effective desorbing agent, particularly at higher concentrations.

The ligand modified with 2-((*E*)-(4-aminophenylimino) methyl) benzoic acid demonstrates strong reusability for removing lead(II) and cadmium(II) from aqueous solutions. Over five sorption–desorption cycles, a slow decline in sorption capacity and elution efficiency is observed, which reflects that, the ligand retains a significant portion of its performance, indicating its practical potential (Table S3†). For Cd(II), the removal tendency ramped down from 51.9 to 47.5 mg g^{-1} (8.5% reduction), while desorption efficiency drops from 95.1% to 86.1% (9.0% reduction). This suggests minor structural changes affecting ion affinity, though the high desorption efficiency confirms the reversible nature of the process. Similarly, Pb(II) uptake affinity declines from 62.1 to 56.7 mg g^{-1} (8.7% reduction), and desorption efficiency drops from 97.1% to 86.9% (10.2% reduction). Overall, the study confirms the ligand's effectiveness for lead(II) and cadmium(II) elimination, making it a highly suitable option for environmental remediation.

3.8. Case study; application in real waste raffinate solution

The application of the synthesized ligand in a real waste solution demonstrates its effectiveness and selectivity for heavy metal removal in complex aqueous matrices. The waste solution, sourced from Cairo Chemical Industries, a private chemical manufacturing company in Egypt, contained a mixture of heavy metals (Pb, Cd, Cr, Co, Si) and common ions (Cl^-, K, Na), with initial concentrations ranging from 70 ppm for Cr to 690 ppm for K (Table S4†). After adsorption under experimental conditions of room temperature, 1.0 g L^{-1} ligand dosage, and 240 minutes shaking time, the final concentrations and removal efficiencies (*E*%) were measured and displayed in Table S4.† The ligand exhibited high selectivity and efficiency for Pb and Cd removal, with removal efficiencies of 62.0% for Pb and 51.1% for Cd. This performance is consistent with the batch, kinetic, and isotherm studies, which highlighted the strong affinity of the ligand for cadmium(II) and lead(II) due to the occurrence of surface active groups (–NH_2, –COOH, and –C=N) that facilitate chemisorption.

In contrast, the removal efficiencies for other metals and ions were significantly lower, with 23% for Cr, 24% for Co, and 14% for Si. Common ions such as Cl^-, K, and Na showed minimal removal, with efficiencies of 3.3%, 2.2%, and 10.7%, respectively. This selectivity is owned to the higer coordination interaction formed between the ligand's functional groups and Pb(II)/Cd(II) ions in comparison with other pollutants. The larger ionic radius and greater electronegativity of cadmium(II) and lead(II) further enhance their interactions with the ligand, making them more effectively removed from the solution.

The results also highlight the ligand's ability to function effectively in the presence of competing ions, which is critical for real-world applications in wastewater treatment. Despite the high concentrations of Cl^-, K, and Na, the ligand maintained a high removal efficiency for Pb and Cd ions, demonstrating its robustness and selectivity. This performance aligns with the desorption investigation, which confirmed the ligand's reusability and regeneration potential, further supporting its suitability for practical applications.

The application of the ligand in real waste solutions underscores its potential for heavy metal removal in complex

Open Access Article. Published on 27 June 2025. Downloaded on 2/9/2026 7:51:31 PM. This article is licensed under a Creative Commons Attribution-NonCommercial 3.0 Unported Licence.

environments, such as industrial wastewater and contaminated groundwater. The high selectivity for Pb and Cd, combined with its ability to operate effectively in the presence of competing ions, makes it a highly suitable option for environmental remediation. These findings, together with the batch, kinetic, isotherm, and thermodynamic results, illuminate a well understanding of the ligand's performance and its potential for real-world implementation.

4. Conclusion

This study successfully demonstrated the potential of 2-((*E*)-(4-aminophenylimino)methyl) benzoic acid as an efficient and selective sorbent for cadmium(II) and lead(II) capture from aqueous solutions. The ligand's unique molecular structure, featuring amino (–NH_2), carboxyl (–COOH), and imine (–C═N) functional groups, enables strong coordination bonding, electrostatic interactions, and chelation with metal ions, resulting in exceptional uptake affinity of 84.0 and 71.0 mg g^{-1} for lead(II) and cadmium(II) respectively. Kinetic and isotherm investigation elucidate that the target ions capture is governed by chemisorption, and the anticipated results are fitting well to pseudo-second-order and Langmuir models. The exothermic and spontaneous nature of the uptake system is explored from the thermodynamic investigation. The ligand demonstrated high selectivity for lead(II) and cadmium(II) over other metals and common ions, as well as excellent reusability over multiple adsorption–desorption cycles, highlighting its potential for practical applications in environmental remediation.

Data availability

All the data used for this work are available upon request.

Author contributions

A. E. Mubark: experimental operation, data interpretation, writing & editing. S. M. El-Gamasy: synthesis, characterization, data curation & interpretation, writing – original draft. A. M. Masoud: experimental operation, data interpretation, writing – reviewing & editing. A. A. El-Zahhar: methodology, validation, data curation & interpretation, writing – original draft, reviewing & editing. M. M. Alghamdi: methodology, validation, data curation & interpretation, writing – original draft. M. H. Taha: characterization, data curation & interpretation, writing – original draft, reviewing & editing. T. F. Hassanein: methodology, validation, data curation & interpretation, writing – original draft, reviewing & editing.

Conflicts of interest

There are no conflicts to declare.

Acknowledgements

The authors express their gratitude to the Deanship of Research and Graduate Studies at King Khalid University for supporting this research through the Large Research Project under grant number RGP 2/74/45.

References

1 T. Liu, Y. Lawluvy, Y. Shi, *et al*) Adsorption of cadmium and lead from aqueous solution using modified biochar: A review, *J. Environ. Chem. Eng.*, 2022, **10**, 106502, DOI: 10.1016/J.JECE.2021.106502.

2 S. Hu, S. Zhang, J. Qin, *et al*) Simultaneous determination of lead and cadmium in water by metal oxide framework complex-modified glassy carbon electrodes, *Microchem. J.*, 2024, **205**, 111154, DOI: 10.1016/J.MICROC.2024.111154.

3 A. K. Tolkou, D. K. Toubanaki and G. Z. Kyzas, Detection of Arsenic, Chromium, Cadmium, Lead, and Mercury in Fish: Effects on the Sustainable and Healthy Development of Aquatic Life and Human Consumers, *Sustain*, 2023, **15**, 16242, DOI: 10.3390/SU152316242.

4 A. E. Mubark, E. G. Zaki, H. A. Hakem, *et al*) Guar Gum Hydrogel as a Biosorbent for Cd(II) and Cu(II) Ions: Kinetic, Equilibrium, and Thermodynamic Insights, *ChemistrySelect*, 2025, **10**, e202404817, DOI: 10.1002/SLCT.202404817.

5 H. A. S. Alhaithloul, I. M. Alsudays, E. S. G. Zaki, *et al*) Retrieval of Cu2+ and Cd2+ ions from aqueous solutions using sustainable guar gum/PVA/montmorillonite nanocomposite films: effect of temperature and adsorption isotherms, *Front. Chem.*, 2024, **12**, 1393791, DOI: 10.3389/FCHEM.2024.1393791/BIBTEX.

6 A. Yousif Rmaidh, A. Salam Al-Mahdawi, N. Sabah Al-Obaidi and M. A. Al-Obaidi, Organic ligands as ligand surface of heavy metals and evaluating antibacterial activity of synthesized complexes, *Inorg. Chem. Commun.*, 2023, **156**, 111148, DOI: 10.1016/J.INOCHE.2023.111148.

7 A. K. H. Hama, F. S. Mustafa, K. M. Omer, *et al*) Heavy metal pollution in the aquatic environment: efficient and low-cost removal approaches to eliminate their toxicity: a review, *RSC Adv.*, 2023, **13**, 17595–17610, DOI: 10.1039/D3RA00723E.

8 S. Siddha and M. Kumar, Sustainable approaches for heavy metal removal from water, *Role Green Chem Ecosyst Restor to Achieve Environ Sustain*, 2024, 227–235, DOI: 10.1016/B978-0-443-15291-7.00023-7.

9 E. Rahmanifar, F. Shiri, S. Shahraki and P. Karimi, Experimental design for removal of lead ions from water samples using an engineered novel chitosan functionalized Schiff-base ligand, *Chem. Eng. Commun.*, 2023, **210**, 2022–2034, DOI: 10.1080/00986445.2023.2174862.

10 A. N. Al-Ghouti, S. S. Al-Maadeed, G. M. Al-Yaqoub, A. Al-Sadi, H. Al-Yafei and A. M. Al-Maadeed, A cost-effective o-toulidine-based Schiff base as an efficient sorbent for metal ion uptake from aqueous and soil samples: Synthesis, antimicrobial, and acute toxicity analyses, *Front. Environ. Sci.*, 2023, **11**, 1128256, DOI: 10.3389/fenvs.2023.1128256.

11 G. S. Nyamato, I. T. Kabogo, S. Maqinana, *et al*) Removal, mechanistic and kinetic studies of Cr(VI), Cd(II), and Pb(II) cations using Fe3O4 functionalized Schiff base chelating

© 2025 The Author(s). Published by the Royal Society of Chemistry

Open Access Article. Published on 27 June 2025. Downloaded on 2/9/2026 7:51:31 PM. This article is licensed under a Creative Commons Attribution-NonCommercial 3.0 Unported Licence.

ligands, *Environ. Sci. Pollut. Res.*, 2024, **31**, 63374–63392, DOI: 10.1007/S11356-024-35443-8/METRICS.

12 M. S. Hussain, S. G. Musharraf, M. I. Bhanger and M. I. Malik, Salicylaldehyde derivative of nano-chitosan as an efficient ligand for lead(II), copper(II), and cadmium(II) ions, *Int. J. Biol. Macromol.*, 2020, **147**, 643–652, DOI: 10.1016/J.IJBIOMAC.2020.01.091.

13 H. Y. Mostafa, A. M. Masoud, A. A. El-Zahhar, *et al*) Amino-alcohol functionalized porous polymer coupled with chromium hydroxide nanoparticles for efficient Cd(ii) adsorption from aqueous solutions, *RSC Adv.*, 2025, **15**, 3480–3496, DOI: 10.1039/D4RA08579E.

14 S. M. Aljubiri, A. A. O. Younes, E. H. Alosaimi, *et al*) Recycling of Sewage Sludge: Synthesis and Application of Sludge-Based Activated Carbon in the Efficient Removal of Cadmium (II) and Lead (II) from Wastewater, *Int. J. Mol. Sci.*, 2024, **25**, 9866, DOI: 10.3390/IJMS25189866.

15 J. Lach and E. Okoniewska, Equilibrium, Kinetic, and Diffusion Mechanism of lead(II) and cadmium(II) Adsorption onto Commercial Activated Carbons, *Mol*, 2024, **29**, 2418, DOI: 10.3390/MOLECULES29112418.

16 I. U. Umoren, S. U. Sunday and S. E. Shaibu, Application of the Langmuir and Freundlich equations for the removal of Cd2++ and Pb2+ ions by adsorption on to natural clay minerals, *World J Appl Sci Technol*, 2023, **15**, 267–274, DOI: 10.4314/WOJAST.V15I2.17.

17 I. U. Umoren and I. O. James, Adsorption characteristics of Zn (ii), Pb (ii) and Cd (ii) ions from aqueous solution onto natural clay minerals, *World J Appl Sci Technol*, 2023, **15**, 347–353, DOI: 10.4314/wojast.v15i2.28.

18 M. S. Hakim, R. M. Iqbal, F. Adany, *et al*) A Review on Development of Porous Aluminosilicate-Based Zeolite Ligand for Heavy Metal Pollution Treatment, *J. Sains. Mater. Indones.*, 2024, **25**, 85–99, DOI: 10.55981/JSMI.2024.1076.

19 Z. Darban, S. Shahabuddin, R. Guar, I. Ahmad and N. Sridewi, Hydrogel-based superadsorbents for efficient removal of heavy metals in industrial wastewater treatment and environmental conservation, *Environ. Funct. Mater.*, 2024, DOI: 10.1016/j.efmat.2024.01.001.

20 D. Fan, Y. Peng, X. He, *et al*) Recent Progress on the Adsorption of Heavy Metal Ions Pb(II) and Cu(II) from Wastewater, *Nanomater*, 2024, **14**, 1037, DOI: 10.3390/NANO14121037.

21 R. Chakraborty, A. Asthana, A. K. Singh, *et al*) Adsorption of heavy metal ions by various low-cost ligands: a review, *Int. J. Environ. Anal. Chem.*, 2022, **102**, 342–379, DOI: 10.1080/03067319.2020.1722811.

22 R. P. Rodríguez, L. Á. Alfonso Herrera, J. M. Cervantes, *et al*) Highly efficient adsorption of aqueous heavy metals by Co-derived metal-organic framework. Synergistic mechanism for enhanced water purification, *J. Solid State Chem.*, 2024, **338**, 124833, DOI: 10.1016/J.JSSC.2024.124833.

23 S. Singh, H. Basu, M. K. T. Bassan and R. K. Singhal, Thiol functionalised silica microsphere loaded polymeric hydrogel: Development of a novel hybrid sorbent for removal of lead and cadmium, *Chemosphere*, 2022, **286**, 131659, DOI: 10.1016/J.CHEMOSPHERE.2021.131659.

24 M. Kaur, S. Kumar, M. Yusuf, *et al*) Schiff base-functionalized metal-organic frameworks as an efficient ligand for the decontamination of heavy metal ions in water, *Environ. Res.*, 2023, **236**, 116811, DOI: 10.1016/J.ENVRES.2023.116811.

25 A. N. A. Hosain, A. El Nemr, A. El Sikaily, *et al*) Surface modifications of nanochitosan coated magnetic nanoparticles and their applications in Pb(II), Cu(II) and Cd(II) removal, *J. Environ. Chem. Eng.*, 2020, **8**, 104316, DOI: 10.1016/J.JECE.2020.104316.

26 A. E. Mubark, S. E. Abd-El Razek, A. A. Eliwa and S. M. El-Gamasy, Investigation on the Sulfadiazine Schiff Base Adsorption Ability of Y(III) Ions from Nitrate Solutions, Kinetics, and Thermodynamic Studies, *Solvent Extr. Ion Exch.*, 2023, **41**, 374–400, DOI: 10.1080/07366299.2023.2186180.

27 N. Wu, A. O. Hall, S. Phadke, *et al*) Adapting Meaningful Learning Strategies for an Introductory Laboratory Course: Using Thin-Layer Chromatography to Monitor Reaction Progress, *J. Chem. Educ.*, 2019, **96**, 1873–1880, DOI: 10.1021/ACS.JCHEMED.9B00256/ASSET/IMAGES/MEDIUM/ED-2019-00256F_0005.GIF.

28 S. M. El-Gamasy, A. E. Mubark, S. E. A. El Razek and A. A. Eliwa, A study on the adequacy of some actinides adsorption on a modified guanidine Schiff base from laboratory effluents, *Can. J. Chem. Eng.*, 2024, DOI: 10.1002/CJCE.25544.

29 F. G. Fahad, S. T. Al-Humairi, A. T. Al-Ezzi, *et al*) Advancements in Liquid Desiccant Technologies: A Comprehensive Review of Materials, Systems, and Applications, *Sustain*, 2023, **15**, 14021, DOI: 10.3390/SU151814021.

30 M. H. Taha, Sorption of U(VI), Mn (II), Cu(II), Zn(II), and Cd(II) from multi-component phosphoric acid solutions using MARATHON C resin, *Environ. Sci. Pollut. Res.*, 2021, **28**, 12475–12489, DOI: 10.1007/S11356-020-11256-3/TABLES/7.

31 M. Mozaffari Majd, V. Kordzadeh-Kermani, V. Ghalandari, *et al*) Adsorption isotherm models: A comprehensive and systematic review (2010–2020), *Sci. Total Environ.*, 2022, **812**, 151334, DOI: 10.1016/J.SCITOTENV.2021.151334.

32 Q. Hu, S. Pang and D. Wang, In-depth Insights into Mathematical Characteristics, Selection Criteria and Common Mistakes of Adsorption Kinetic Models: A Critical Review, *Sep. Purif. Rev.*, 2022, **51**, 281–299, DOI: 10.1080/15422119.2021.1922444.

33 M. E. González-López, C. M. Laureano-Anzaldo, A. A. Pérez-Fonseca, *et al*) A Critical Overview of Adsorption Models Linearization: Methodological and Statistical Inconsistencies, *Sep. Purif. Rev.*, 2022, **51**, 358–372, DOI: 10.1080/15422119.2021.1951757.

34 P. T. Tho, H. T. Van, L. H. Nguyen, *et al*) Enhanced simultaneous adsorption of As(iii), Cd(ii), Pb(ii) and Cr(vi) ions from aqueous solution using cassava root husk-

Open Access Article. Published on 27 June 2025. Downloaded on 2/9/2026 7:51:31 PM. This article is licensed under a Creative Commons Attribution-NonCommercial 3.0 Unported Licence.

derived biochar loaded with ZnO nanoparticles, *RSC Adv.*, 2021, **11**, 18881–18897, DOI: 10.1039/D1RA01599K.

35 R. Sharma, A. Sarswat, C. U. Pittman and D. Mohan, Cadmium and lead remediation using magnetic and non-magnetic sustainable biosorbents derived from Bauhinia purpurea pods, *RSC Adv.*, 2017, **7**, 8606–8624, DOI: 10.1039/C6RA25295H.

36 X. Chen, M. F. Hossain, C. Duan, *et al*) Isotherm models for adsorption of heavy metals from water - A review, *Chemosphere*, 2022, **307**, 135545, DOI: 10.1016/J.CHEMOSPHERE.2022.135545.

37 M. H. Taha, A. M. Masoud, Y. M. Khawassek, *et al*) Cadmium and iron removal from phosphoric acid using commercial resins for purification purpose, *Environ. Sci. Pollut. Res.*, 2020, **27**, 31278–31288, DOI: 10.1007/S11356-020-09342-7/TABLES/4.

38 A. M. Masoud, A. E. Mubark, M. H. Taha and S. Ibrahim, Nanostructured layered double hydroxide (NLDH) – Zn/Al-based materials: strategy to improve performance for zirconium sorption from acidic sulfate solution, *RSC Adv.*, 2024, **14**, 28455–28468, DOI: 10.1039/D4RA03845B.

39 M. Maslova, V. Ivanenko, N. Yanicheva and L. Gerasimova, The effect of heavy metal ions hydration on their sorption by a mesoporous titanium phosphate ion-exchanger, *J. Water Process Eng.*, 2020, **35**, 101233, DOI: 10.1016/J.JWPE.2020.101233.

40 M. Sridhar, G. Ravi, K. L. Reddy, P. M. Reddy, P. Ramesh and A. K. Raju, Synthesis of Co(II) Metal Complexes of Tryptanthrin Schiff Bases, Characterization, their Biological Evaluation, and Molecular Docking Studies, *Asian J. Green Chem.*, 2024, **8**(4), 441–456, DOI: 10.22034/ajgc.2024.199083.

41 W. A. Mahmoud, Z. M. Hassan and R. W. Ali, Synthesis and spectral analysis of some metal complexes with mixed Schiff base ligands 1-[2-(2-hydroxybenzylideneamino)ethyl] pyrrolidine-2,5-dione (HL1) and (2-hydroxybenzalidine) glycine (HL2), *J. Phys.:Conf. Ser.*, 2020, **1660**, 012027, DOI: 10.1088/1742-6596/1660/1/012027.

42 H. Y. Sharef and N. A. Fakhre, Rapid adsorption of some heavy metals using extracted chitosan anchored with new aldehyde to form a schiff base, *PLoS One*, 2022, **17**, e0274123, DOI: 10.1371/JOURNAL.PONE.0274123.

43 S. Parambadath, A. Mathew, A. Mohan and C. S. Ha, Chelation dependent selective adsorption of metal ions by Schiff Base modified SBA-15 from aqueous solutions, *J. Environ. Chem. Eng.*, 2020, **8**, 104248, DOI: 10.1016/J.JECE.2020.104248.

44 A. Vázquez-Guerrero, R. Cortés-Martínez, R. Alfaro-Cuevas-villanueva, *et al*) Cd(II) and Pb(II) Adsorption Using a Composite Obtained from Moringa oleifera Lam. Cellulose Nanofibrils Impregnated with Iron Nanoparticles, *Water*, 2021, **13**, 89, DOI: 10.3390/W13010089.

45 M. D. Meitei and M. N. V. Prasad, Lead (II) and cadmium (II) biosorption on Spirodela polyrhiza (L.) Schleiden biomass, *J. Environ. Chem. Eng.*, 2013, **1**, 200–207, DOI: 10.1016/J.JECE.2013.04.016.

46 M. Solic, S. Maletic, M. K. Isakovski, *et al*) Removing low levels of Cd(II) and Pb(II) by adsorption on two types of oxidized multiwalled carbon nanotubes, *J. Environ. Chem. Eng.*, 2021, **9**, 105402, DOI: 10.1016/J.JECE.2021.105402.

47 B. Cao, J. Qu, Y. Yuan, *et al*) Efficient scavenging of aqueous Pb(II)/Cd(II) by sulfide-iron decorated biochar: Performance, mechanisms and reusability exploration, *J. Environ. Chem. Eng.*, 2022, **10**, 107531, DOI: 10.1016/J.JECE.2022.107531.

48 I. Abouda, S. Walha, S. Bouattour, *et al*) Cotton fabric functionalized with nanostructured MoS_2: Efficient ligand for removal of Pb, Hg, Cd and Cr from water, *J. Environ. Chem. Eng.*, 2022, **10**, 108583, DOI: 10.1016/J.JECE.2022.108583.

49 X. Liu, R. Tian, W. Ding, *et al*) Adsorption selectivity of heavy metals by Na-clinoptilolite in aqueous solutions, *Adsorption*, 2019, **25**, 747–755, DOI: 10.1007/S10450-019-00081-X/FIGURES/7.

50 F. Dhaouadi, L. Sellaoui, H. E. Reynel-Ávila, *et al*) Adsorption mechanism of Zn2+, Ni2+, Cd2+, and Cu2+ ions by carbon-based ligands: interpretation of the adsorption isotherms *via* physical modelling, *Environ. Sci. Pollut. Res.*, 2021, **28**, 30943–30954, DOI: 10.1007/S11356-021-12832-X/FIGURES/9.

51 Z. Chu, W. Gu and Y. Li, Adsorption mechanism of heavy metals in heavy metal/pesticide coexisting sediment systems through factional factorial design assisted by 2D-QSAR models, *Pol. J. Environ. Stud.*, 2018, **27**, 2451–2462, DOI: 10.15244/PJOES/80962.

52 M. Rahm, R. Hoffmann and N. W. Ashcroft, Atomic and Ionic Radii of Elements 1–96, *Chem. –Eur. J.*, 2016, **22**, 14625–14632, DOI: 10.1002/CHEM.201602949.

53 M. Medykowska, M. Wiśniewska, K. Szewczuk-Karpisz and R. Panek, Interaction mechanism of heavy metal ions with the nanostructured zeolites surface – Adsorption, electrokinetic and XPS studies, *J. Mol. Liq.*, 2022, **357**, 119144, DOI: 10.1016/J.MOLLIQ.2022.119144.

54 X. Fan, H. Liu, E. Anang and D. Ren, Effects of Electronegativity and Hydration Energy on the Selective Adsorption of Heavy Metal Ions by Synthetic NaX Zeolite, *Mater*, 2021, **14**, 4066, DOI: 10.3390/MA14154066.

55 F. Noun, E. A. Jury and R. Naccache, Elucidating the Quenching Mechanism in Carbon Dot-Metal Interactions–Designing Sensitive and Selective Optical Probes, *Sensors*, 2021, **21**, 1391, DOI: 10.3390/S21041391.

56 M. Dudev, J. Wang, T. Dudev and C. Lim, Factors governing the metal coordination number in metal complexes from cambridge structural database analyses, *J. Phys. Chem. B*, 2006, **110**, 1889–1895, DOI: 10.1021/JP054975N/SUPPL_FILE/JP054975NSI20050902_074636.

57 Y. Xia, G. Liao, Z. Wang, *et al*) Efficient and deep adsorption of thallium(I) from complex water based on hard-soft acid-base theory, *Sep. Purif. Technol.*, 2025, **360**, 131221, DOI: 10.1016/J.SEPPUR.2024.131221.

58 M. El Hefnawy, A. F. Shaaban and H. A. Elkhawaga, Effective removal of Pb(II), Cd(II) and Zn(II) from aqueous solution by a novel hyper cross-linked nanometer-sized chelating resin, *J. Environ. Chem. Eng.*, 2020, **8**, 103788, DOI: 10.1016/J.JECE.2020.103788.

© 2025 The Author(s). Published by the Royal Society of Chemistry

Open Access Article. Published on 27 June 2025. Downloaded on 2/9/2026 7:51:31 PM.
This article is licensed under a Creative Commons Attribution-NonCommercial 3.0 Unported Licence.

59 A. A. Taha, M. A. Shreadah, A. M. Ahmed and H. F. Heiba, Multi-component adsorption of Pb(II), Cd(II), and Ni(II) onto Egyptian Na-activated bentonite; equilibrium, kinetics, thermodynamics, and application for seawater desalination, *J. Environ. Chem. Eng.*, 2016, **4**, 1166–1180, DOI: **10.1016/J.JECE.2016.01.025**.

60 A. N. Ebelegi, N. Ayawei, D. Wankasi, *et al*) Interpretation of Adsorption Thermodynamics and Kinetics, *Open J. Phys. Chem.*, 2020, **10**, 166–182, DOI: **10.4236/OJPC.2020.103010**.

61 A. K. Priya, V. Yogeshwaran, S. Rajendran, *et al*) Investigation of mechanism of heavy metals (Cr6+, Pb2+& Zn2+) adsorption from aqueous medium using rice husk ash: Kinetic and thermodynamic approach, *Chemosphere*, 2022, **286**, 131796, DOI: **10.1016/J.CHEMOSPHERE.2021.131796**.

62 L. Joseph, M. Saha, S. Kim, *et al*) Removal of Cu2+, Cd2+, and Pb2+ from aqueous solution by fabricated MIL-100(Fe) and MIL-101(Cr): Experimental and molecular modeling study, *J. Environ. Chem. Eng.*, 2021, **9**, 106663, DOI: **10.1016/J.JECE.2021.106663**.

63 F. Ge, M. M. Li, H. Ye and B. X. Zhao, Effective removal of heavy metal ions Cd2+, Zn2+, Pb2+, Cu2+ from aqueous solution by polymer-modified magnetic nanoparticles, *J. Hazard. Mater.*, 2012, **211**(212), 366–372, DOI: **10.1016/J.JHAZMAT.2011.12.013**.